1DVAR analysis of temperature and humidity using GPS radio occultation data

Paul Poli[1,4], Joanna Joiner[2], Emil Robert Kursinski[3]

April 20, 2000

Short title: 1DVAR WITH GPS R.O. DATA

1DVAR ANALYSIS OF TEMPERATURE AND HUMIDITY USING GPS RADIO OCCULTATION DATA

Paul Poli[1,4]*, Joanna Joiner[2], Robert Kursinski[3]

[1]Joint Center for Earth Systems Technology, Baltimore, Maryland, USA
[2]Data Assimilation Office, NASA Goddard Space Flight Center, Greenbelt, Maryland, USA
[3]Jet Propulsion Laboratory, Pasadena, California, USA
[4]also at Météo-France, Toulouse, France

The Global Positioning System enables positioning in 3 dimensions about our planet. It has been operationnal since 1994. Twenty-four satellites are used to achieve this performance. The signals sent by these satellites are electromagnetic waves travelling through our atmosphere down to the small receivers used by the civilian community and the military.

Because of varying meteorological conditions (namely temperature and humidity changes along the ray path), the rays do not travel in a straight line. They bend towards the surface. As a consequence, the ray path between two points is longer than a straight line, and the time it takes for a signal to travel this distance is longer.

In 1995, a small GPS receiver was launched on a satellite (GPS/MET). It became possible to perform radio occultations around the Earth: the source - one of the 24 GPS satellites - is seen by the receiver as it rises or sets around the other side of the Earth. When the source disappears, the receiver progressively loses the signals. By measuring accurately the time delay between the emission and the reception of the signal, it is possible to infer which part of the delay is due to the atmosphere.

We use GPS/MET data to retrieve temperature and humidity profiles simultaneously. A specific method is implemented : it combines information from numerical forecasts and GPS observations in an optimal way. Comparing the result with an independent source of observations (weather balloons), we demonstrate that GPS data have the potential to improve weather analyses. We also show that improved temperature and humidity profiles can be obtained using information from a forecast model. This confirms results obtained in this study using simulated data.

*Corresponding author address: Paul Poli, Code 910.3, NASA/GSFC, Greenbelt, MD 20771. e-mail: ppoli@dao.gsfc.nasa.gov

Abstract.

The Global Positioning System (GPS) employs a constellation of satellites which provide a stable source of electromagnetic signals available for radio occultation purposes about our planet. The atmospheric-induced bending of the rays can be converted into refractivity profiles for each occultation. We implement here a one-dimensional variational (1DVAR) analysis which enables retrieving both temperature and humidity profiles without ambiguity.

We perform a linear error analysis study and a fully non-linear Monte-Carlo simulation. They both show the potential impact of the GPS to improve upon an accurate first guess from a data assimilation system. The information content of the GPS soundings is significant at all latitudes for temperature, and only in the tropics for humidity.

1DVAR retrievals based on real data collected during the GPS/MET experiment in 1995 are validated against radiosondes. They show an excellent capacity of the GPS measurements to resolve the tropopause.

In the northern hemisphere and in the tropics, we demonstrate a net reduction of temperature bias and standard deviation, as compared with the Goddard Earth Observing System (GEOS) model background information used to constrain the profiles. The results show that an analysis using GPS refractivity can yield significant improvement over the background at a relatively small computing cost, and in spite of the spherical symmetry assumption used to derive refractivity from the GPS measurements. We also show that a 1DVAR yields better results than a direct retrieval method in which a temperature (humidity) profile is assumed to be the truth in order to retrieve a humidity (temperature) profile. Finally, we point out significant sensitivities of the retrievals to the gravitational constant, the surface pressure and the number of levels used to perform the analysis.

This represents a step towards using the GPS data to improve NWP forecasts.

1. Introduction

The Global Positioning System (GPS) system enables positioning in 3 dimensions on our planet. Its radio signals are sensitive to the atmosphere. This makes it possible to perform soundings using the radio occultation technique (RO). This approach has been used at NASA for more than thirty years to study the atmospheres of other planets [e.g. *Lindal*, 1992]. *Gorbunov and Sokolovskiy* [1993] provided simulations of GPS radio occultation measurements. *Kursinski et al.* [1997] also simulated many aspects of GPS measurements and their expected error characteristics. GPS/MET (1995) was the first radio occultation experiment conducted on Earth using that technique [e.g. *Kursinski et al.*, 1996].

Before using the GPS data in a data assimilation system for numerical weather prediction (NWP) or climate study, a first step is to appraise the impact these data have on the analysis. One technique for assessing impact is the Observing System Simulation Experiment (OSSE). *Kuo et al.* [1998] have performed OSSE's with simulated GPS data. There are known limitations of OSSE's [*Atlas*, 1997] and therefore care must be taken when interpreting the results. For example, no observation errors were included in the *Kuo et al.* [1998] OSSE. We will give an example of the effect of neglecting errors in a simulation.

In this work, both simulated and real observations are analyzed to gauge the impact of GPS data on an analysis. For this purpose, we have developed a one dimensional variational (1DVAR) analysis. In this approach, background information from a General Circulation Model (GCM) forecast is used to constrain the retrievals. Analyzed temperature and humidity are obtained without ambiguity. The approach also yields an estimate of the errors, based on the assumed observation and background errors.

The outline of the paper is as follows : First we give a description of the GPS. Next, the radio occultation technique is described. We discuss the different possible approaches to retrieve and assimilate atmospheric properties from GPS measurements. Then, we describe the implementation of a 1DVAR analysis of refractivity. After this, we show results of a Monte-Carlo simulation and linear error analysis. We then discuss some unexpected sensitivities of the GPS analyses. Finally, we validate GPS/MET 1DVAR retrievals using collocated radiosondes.

2. The Global Positioning System

The GPS was designed by the U.S. Department of Defense (USDoD). Its main purpose is to aid in navigation. It has enabled accurate positioning anywhere about the globe since 1994. It consists of 24 orbiting satellites distributed in six orbital planes. The 20,200 km orbits are circular with an inclination of 55° and a period of 12 hours. The principle of the GPS is based on the path delay of a propagating radio signal. Two L-band frequencies are used : L_1 1575.42 MHz (or 19.0 cm) and L_2 1227.60 MHz (or 24.4 cm).

The accuracy of GPS measurements is intentionally degraded by encryption for security reasons. This is known as "selective availability". First-generation receivers were launched on GPS/MET (1995) and Øersted (1999). Their ability to track the occultations is degraded when the encryption is on, which is generally the case except during very short periods for scientific studies. Second-generation GPS receivers built for the purposes of the radio occultation are to be flown on the upcoming missions Champ (Germany) and SAC-C (Argentina). These receivers are able to better process encoded signals, for which the L_2 signal-to-noise (SNR) ratio is very low.

An exact positioning cannot be achieved for several reasons [*Doerflinger*, 1998]. First, the exact position and velocity of the GPS satellites must be known perfectly (at a given time) to position a receiver relative to them. It follows that (1) orbit errors (2) clock drifts (3) relativistic effects (4) receiver system errors (antenna and receiver noise) and (5) use of approximate co-ordinates contribute to the total error of the measurement. Other perturbations in signals that degrade the quality of the positioning for a terrestrial receiver are caused by atmospheric refraction and scattering which may cause multipath effects.

The applications of GPS to meteorology include positioning *in situ* measurements, computing wind speed from the drift of radiosondes, and measuring the total column of water vapor above a ground-based receiver [e.g. *Bevis et al.*, 1992, *Elgered et al.*, 1997]. In this study, we focus on space-based GPS receivers.

3. Radio Occultation with GPS

3.1. Assets of the GPS Radio Occultation Technique

There are several positive attributes of GPS occultations as an atmospheric sounding device. A high-inclination LEO provides a set of observations that covers the globe fairly uniformly at a relatively low cost [*Yunck et al.*, 1988]. The GPS coverage anywhere about the globe is advantageous when comparing to that obtained from balloon-launched radiosondes (about 800 each 12 hours, the majority over the northern hemisphere continents). A single GPS receiver may optimally obtain approximately 500 occultations per day [*Kursinski et al.*, 1997].

When compared within IR spaceborne sounders, the radio occultation (RO) technique with GPS has the advantage of being an "all-weather" system. It is relatively insensitive to aerosols, cloud or rain, due to wavelengths of order 20 cm. Unlike other techniques the GPS radio occultation provides a degree of self-calibration because relative phase shifts are the relevant information. Moreover, the stability of the transmitters limits temporal drifts.

Finally, due to its limb-viewing geometry, the GPS RO has a higher vertical resolution (~1.5 km) than passive nadir sounders. This resolution is more comparable to radiosondes. Furthermore, the ratio between vertical and horizontal resolution (about 300 km) is consistent with that of quasi-geostrophic flows [*Lindzen and Fox-Rabinovitz*, 1989; *Kursinski et al.*, 1997].

3.2. Configuration of a GPS Occultation

Figure 1 shows the configuration of a GPS occultation. Three transmitters are used for positioning. One transmitter is used for clock correction. A fifth transmitter is used for the occultation. The rays from the source (occulted transmitter) traverse the Earth's atmospheric limb to reach the receiver.

Figure 1

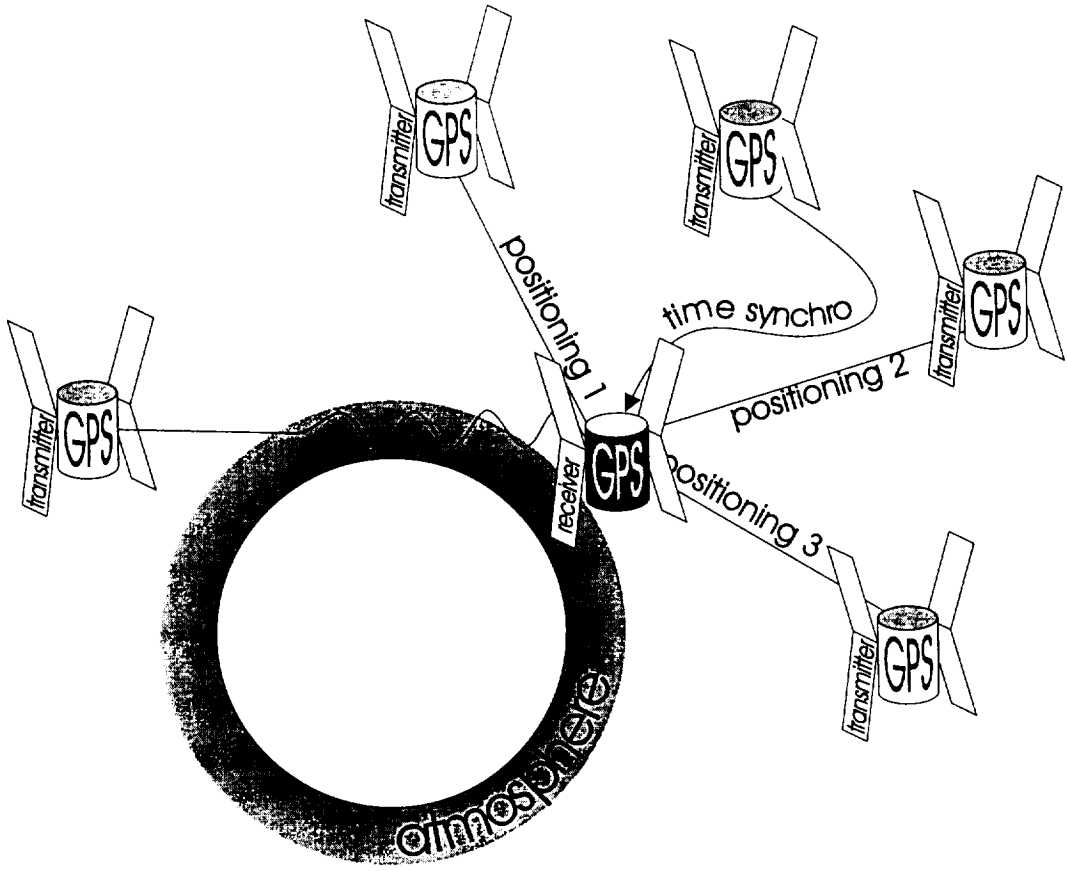

Figure 1. Radio occultation technique applied to GPS

3.3. Bending Effect and Vertical Scanning

Whenever an electromagnetic signal passes through the atmosphere, it is refracted according to Snell's law, due to the vertical gradient of refractivity. This bending lengthens the ray path as compared with the straight path that would be obtained in a vacuum. Because the refractive index is not unity, the waves also travel slower than they would in a vacuum. The latter is more important in terms of delay than the bending. Finally, the GPS signal is affected by atmospheric absorption and scattering. For L-band (large) wavelengths, the scattering effect may be neglected with realistic liquid water and ice contents [*Kursinski et al.*, 1995].

At radio frequencies, it is not possible to make direct and accurate measurements of the refracted angle. However, if the two satellites are in relative motion, the refraction introduces a change in the

Doppler shift of the received signal. After removal of the phase change due to the relative motion of the LEO with respect to the GPS, proper calibration of receiver and transmitter clocks, the extra phase change induced by the atmosphere can be isolated.

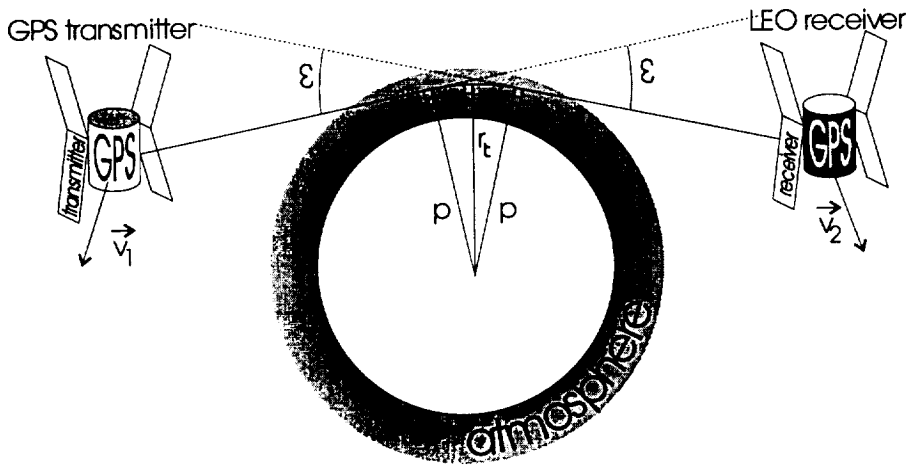

Figure 2. Geometry of a GPS occultation

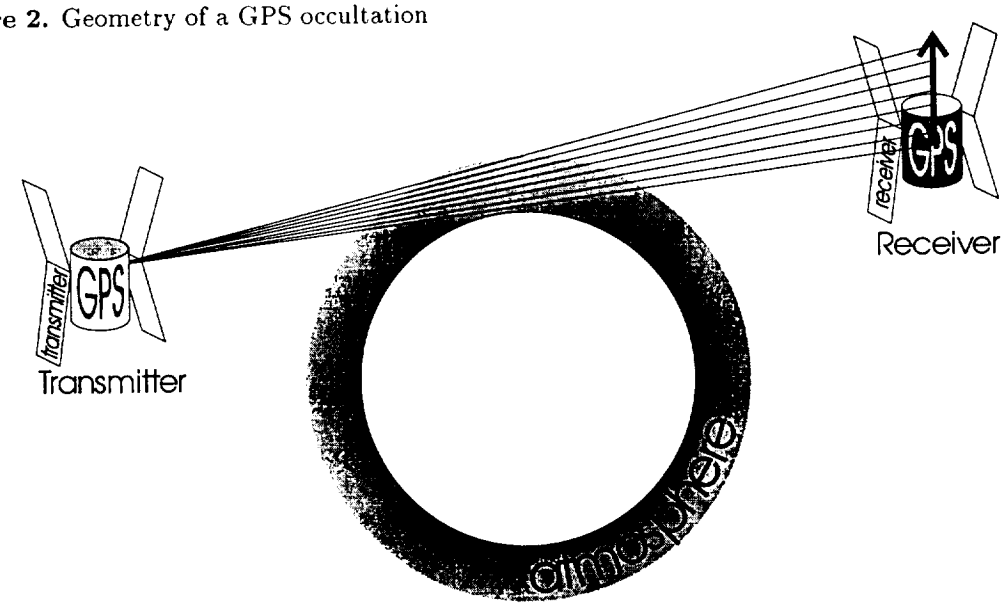

Figure 3. Vertical scanning of the atmosphere during an occultation

The overall effect of the atmosphere can be summed up by a total bending angle ε and an asymptotic ray-miss distance p (commonly called impact parameter), as shown in figure 2. The distance

figure 2

between the perigee point and the center of curvature is r_t. The vertical scanning of the atmosphere is provided by the relative motion between the two orbiting satellites, as depicted in figure 3. Time dependency of both ε and p can be derived from accurate measurements of Doppler-shifted frequency.

figure 3

3.4. Inversion of Bending Angles to Refractivity

The bending induced by the atmosphere ranges approximately between $(2\times10^{-5})°$ at 80 km altitude and 1° nearby the surface [*Kursinski et al.*, 1997]. The horizontal path covered by this bending is about 200~300 km long and 1.5~3 km wide, centered on the tangent point (see figure 4). A typical occultation lasts between 1 and 2 minutes.

figure 4

The variation of refractive index n along a limb path in the Earth's atmosphere is dominated by the vertical gradient. To the first order, the refractive index field is spherically symmetric. If p is the impact parameter for the tangent ray whose radius is r, the bending angle ε can be expressed by :

$$\varepsilon(p) = -2p\int_p^\infty \left(\frac{\partial \ln n}{\partial x}\right)_\theta (x^2-p^2)^{-\frac{1}{2}}\,dx, \tag{1}$$

where $x = rn$ [e.g. *Eyre*, 1994]. An elegant and direct way to obtain n from ε and p is to use Abelian transformation assuming a local spherical symmetry, i.e. :

$$n(x) = \exp\left[\frac{1}{\pi}\int_x^\infty \varepsilon(p)\,(p^2-x^2)^{\frac{1}{2}}\,dp\right], \tag{2}$$

[e.g. *Eyre*, 1994].

Errors in computing n by this approach result from (1) local spherical asymmetry, (2) non-coplanar rays, (3) non-vertical scanning (because both satellites drift during an occultation [*Eyre*, 1994]) and (4) an inaccurate upper boundary used to initiate the integral [*Steiner et al.*, 1999]. The integral formulation of the Abel transform spreads the errors in this boundary condition along the vertical and smoothes the observed bending angles variations. Consequently, the computed refractivity cannot reproduce the full sharpness of derived bending angles.

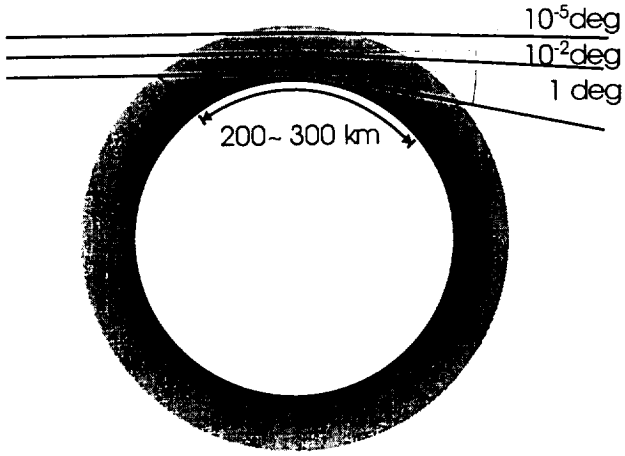

Figure 4. Bending of the rays during an occultation

3.5. Interpretation of Refractivity

For microwave frequencies, the refractivity N (defined by $N = 10^6 (n - 1)$) of the atmosphere can be expressed by :

$$N = b_1 \frac{P}{T} + b_2 \frac{P_w}{T^2} + b_3 \frac{N_e}{f^2} + b_4 W, \tag{3}$$

[e.g. *Kursinski et al.*, 1997] where f is the frequency of the signal emitted by the transmitter in Hz, P the pressure of air (dry air and water vapor) in hPa, T the temperature in K, P_w the partial pressure in water vapor in hPa, N_e the electrons density in m^{-3}, and W the particulates density (primarily liquid water) in $g{\cdot}m^{-3}$. The b_i are constants; b_1 = 77.6 N-unit·K·hPa^{-1}, $b_2 = 3.73{\times}10^5$ N-unit·K^2·hPa^{-1}, $b_3 = 40.3{\times}10^6$ N-unit·Hz^2·m^3, b_4 = 1.4 N-unit·g^{-1}·m^3.

The four refractivity terms in equation 3 are often refered to as (1) hydrostatic (or dry), (2) moist, (3) ionospheric and (4) scattering terms, respectively. The first term is due to the polarizability of atmospheric molecules. It is dominant below 60~90 km. The second term is due to the fact that the water molecule is polar. The ionospheric term results from the free electrons of the ionosphere. It can be removed by the use of the two GPS frequencies f_1 and f_2 [*Kursinski et al.*, 1997]. The last term can

be neglected, as explained in section 3.3. Therefore, after removing the ionospheric component, N can be approximated by [e.g. *Bean and Dutton*, 1968] :

$$N = b_1 \frac{P}{T} + b_2 \frac{P_w}{T^2}. \tag{4}$$

4. Use of GPS for Atmospheric Retrievals and Data Assimilation

There are commonly three levels of GPS radio occultation data available for data assimilation [*Zou et al.*, 1999]: (1) bending angles, (2) refractivity and (3) retrieved profiles of temperature or water vapor. To be assimilated, each level requires an estimate of the errors and an observation operator.

4.1. Assimilation of Bending Angles

These are considered as the "rawest" data (even though Doppler shifts themselves are even rawer data). An estimate of the error in each refracted angle measurement is needed. The advantage of using these data is that, at each point, the observation errors are mostly uncorrelated with respect to each other.

However, the observation operator is quite complex [*Eyre*, 1994]. First, it has to interpolate the background information (typically gridded fields from a numerical weather prediction model) for temperature, humidity and pressure to each measurement location. This requirement stands for all approaches. Second, it has to compute the refracted angle ε and its tangent linear model (or adjoint) for a given value of an impact parameter p. This implies computing the derivative of the local refractivity at each point, which is subject to high variability.

Full ray-tracing codes have been developed by *Mortensen and Høeg* [1998] and *Zou et al.* [1999]. They both have the capability to reconstruct the ray path and simulate the overall bending angle from a given state of atmosphere. However, assimilating 30 profiles with a ray-tracing model in the National Centers for Environmental Prediction Data Assimilation System (NCEP-DAS) requires approximately

4 hours of CPU (Central Processing Unit) on a Cray C-90 computer [*Matsumura et al.*, 1999].

Another approach consists of assuming spherical symmetry. Such one-dimensional operators have been developed by *Healy* [1998] and *Palmer* [1998]. The cost is significantly lower than a full ray-tracing. Like the 3D approach, it still involves local derivatives of refractivity.

4.2. Assimilation of Retrieved Profiles of Refractivity

In this approach, the bending angles have to first be inverted with an Abel transform to obtain profiles of refractivity as a function of altitude. The observation operator calculates refractivity from interpolated model variables using (4). This is much simpler and less computationally burdensome than simulating bending angles.

The drawback to this approach is that additional errors are introduced as described in section 3.4. The *main point* is that errors are correlated along the vertical. These errors need to be estimated for accurate assimilation.

4.3. Assimilation of Retrieved Profiles of Temperature and/or Humidity

The retrieval error can be separated into three components [*Rodgers*, 1990] : (1) random error due to measurement noise (2) systematic error due to uncertain model parameters and inversion model bias (3) null-space error due to the inherent finite vertical resolution of the observing system (this is actually the background error component). The *main point* is that temperature and humidity errors in the retrievals are correlated both vertically and horizontally. These errors are difficult to estimate.

The simplicity of such an approach is that the data to be assimilated are essentially the same as those used in a NWP model. Therefore, the observation operator is trivial.

4.4. Summary on the Various Approaches

Bending angles have the simplest error but the most complicated and expensive observation operator. Conversely, retrieved temperature or humidity profiles have the simplest observation operator, but the most complicated errors. The errors accumulate all the approximations made during the

conversion of raw GPS data into meteorological values. Assimilating refractivity represents a good alternative. It has a relatively low computing cost.

The approach chosen here is to retrieve both temperature and humidity in a one-dimensional (1D, over the vertical) 'off-line' analysis based on a model forecast first guess and refractivity measurements. In the next chapter, the one-dimensional variational (1DVAR) analysis scheme is described.

5. GPS-1DVAR Implementation

5.1. Variational Theory

The application of variational analysis to the retrieval of geophysical parameters has been discussed extensively by several authors [e.g. *Rodgers*, 1976, *Eyre*, 1993]. We try to minimize a cost function $\mathcal{J}$ with respect to a variable state of atmosphere x (state vector). This function is

$$\mathcal{J}[x] = (h(x) - y^0)^T R^{-1}(h(x) - y^0) + (x - x^b)^T B^{-1}(x - x^b), \tag{5}$$

[e.g. *Jazwinski*, 1970] where y^0 is the observation vector. h is the observation operator (non-linear), x^b is the background information (for example a 6-hour forecast). R is the error-covariance matrix of the observations, and B is the error-covariance matrix of the background. Hence $h(x)$ is an estimate of the observations that would be made with a state of the atmosphere x. We assume the background and observation errors to be unbiased and uncorrelated with each other.

The minimum variance problem can be solved using a quasi-Newton iteration, *i.e.*,

$$x_{i+1} = x^b + \left(H_i^T R^{-1} H_i + B^{-1}\right)^{-1} H_i^T R^{-1} \left(y^0 - h\left(x\right) + H_i\left(x_i - x^b\right)\right), \tag{6}$$

[e.g. *Rodgers*, 1976] where the subscript i denotes the iteration number, H_i is the tangent linear model of the observation operator h, or Jacobian, and H_i^T the adjoint. We define convergence as the iteration at which the quantity $\mathcal{J}\left[x_i\right]$ has not changed by more than 2% from the previous iteration. In the dataset we used, this distance at convergence is in the mean equal to about two times the number of GPS observations used to resolve one occultation. *Healy et al.* [2000] and *Palmer et al.* [2000] have found this parameter can be used to quality control the GPS observations.

The state vector contains conventional meteorological variables on several pressure levels. After convergence, it represents a solution (the *analysis*) that has an optimal position with respect to both the observations and the background information. These distances, formally expressed in $\mathcal{J}$, are normalized and weighted by the inverse of the matrices R and B, respectively. They represent physical constraints that help choose a solution among the infinite number of possible atmospheric temperature and humidity profiles that would match the observations.

5.2. The State Vector

The state vector includes the temperature and negative of the log of the specific humidity at the background pressure levels. The sea level pressure was added to the state vector as a supplementary degree of freedom. To reduce computational cost, the amount of humidity is taken as equal to a very small value (10^{-9}) and removed from the state vector above a specified level (50 hPa).

In the implementation, the state vector extends only to the lowest perigee point of the occultation. If n is the total number of levels, and n_{P_w} the number of model levels with water vapor in the state variable, the state vector x contains ($n_T = n + n_{P_w} + 1$) elements :

$$x = (T_1, T_2, \ldots, T_n, -\log q_1, -\log q_2, \ldots, -\log q_{n_{P_w}}, P_{sealevel}) \,. \tag{7}$$

5.3. Background Information

We used two sets of background information from the Goddard Earth Observing System (GEOS) model for our analysis. Both included upper stratospheric levels (GEOS-Strat). One set was a 6-hour forecast. Available archived data were specified on 18 selected pressure levels (surface up to 0.4 hPa). The other set was the 'assimilation' product on the 46 σ levels of the General Circulation Model (GCM) from the surface up to 0.1 hPa. The Data Assimilation Office Data Assimilation System (DAO-DAS) uses an Incremental Analysis Update (IAU) approach [*Bloom et al.*, 1996]. It consists of applying gradual increments within the 6-hour assimilation window. The result of this operation in the middle of the window is called the 'assimilation'. So the assimilation background we used already included some

information from the observations (especially radiosondes).

The background error-covariance matrix uses variances from *Joiner and Rokke* [2000]. For temperature, it includes inter-level correlations through the following formula :

$$Cov(T_i, T_j) = \sigma_{T_i}\sigma_{T_j} \exp^{-(\frac{\log(P_i/P_j)}{\Delta L})^2} \exp^{-(\frac{T_i - T_j}{\Delta L \Delta T})^2}, \quad (8)$$

where $Cov(T_i, T_j)$ expresses the temperature error covariance between two levels i and j, σ_{T_i} is the temperature standard deviation for the pressure level P_i, T_i is the temperature at that level, $\Delta L = 0.1$ and $\Delta T = 30$ are constants which were empirically adjusted. Two levels close in log of pressure and temperature will be considered as having highly-correlated errors. Also, in order to take into account the variable altitude of the tropopause, we added a feature to the scheme to fit the local maximum of model error to the altitude of the minimum of temperature. Figure 5 shows the diagonal of the background error covariance matrix for temperature.

Figure 5

The assumed errors are relatively small. However, we did an experiment in which we multiplied the temperature errors by a factor 1.4. The results obtained by comparison with radiosondes (as shown later) were unchanged. The cost function $\mathcal{J}$ at convergence was increased.

The values for humidity variances are listed in Table 1. They were slightly modified from *Joiner and Rokke*. [2000] after optimization by experiments. For the inter-level correlation only the term representing the exponential decrease related to the vertical distance between two levels in (8) is taken into account.

Table 1

We assume a sea level pressure standard deviation of 2.5 hPa. Background temperature, humidity, and sea level pressure errors are assumed to be uncorrelated.

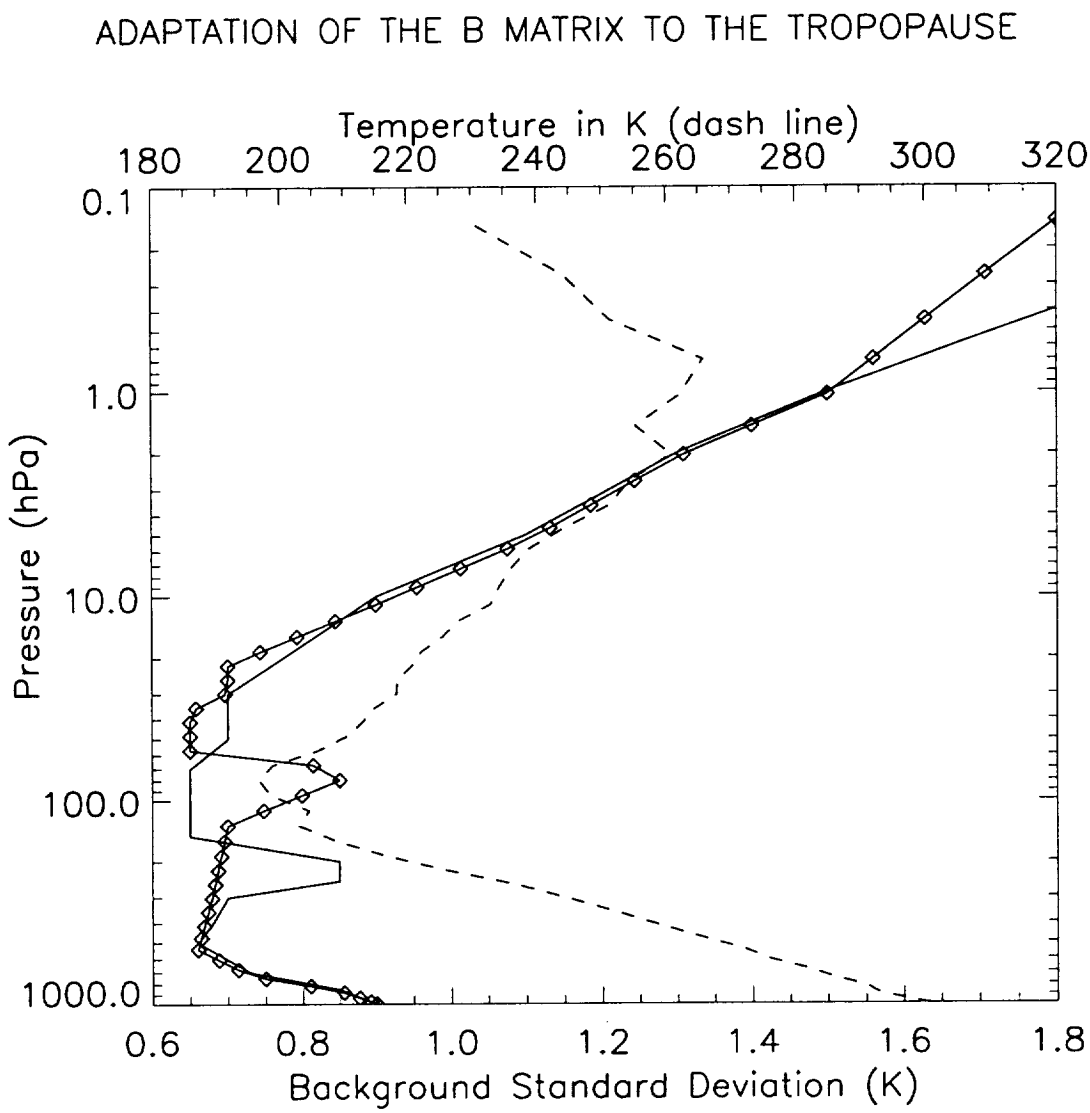

Figure 5. Assumed temperature errors for the background : *plain line* : for a tropopause at 250 hPa (typically mid and high latitudes) - *diamonds* : for the temperature profile with *dashes* (latitude 7°N).

Table 1. Assumed log of specific humidity errors for the background.

Pressure (hPa)	1000	850	700	500	400	300	250	200	150 and beyond
Log(q) std. dev.	0.40	0.40	0.40	0.20	0.25	0.30	0.45	0.60	0.70

5.4. The GPS Observations

During the GPS/MET mission, there were some time periods when the Anti-Spoofing (A/S) encryption was turned off by the USDoD. We used the data from one of these, called 'Prime Time 2' from June 21st to July 4th 1995. The dataset, a total of 797 occultations, is shown in figure 6.

figure 6

We assumed the following errors in the refractivity data : 1% below 5 km, 0.2% up to 30 km. They follow the estimations of *Kursinski et al.* [1997]. Above 30 km, several sources of error, negligible in the troposphere, become gradually more important as the refractivity becomes very small [*Kursinski et al.*, 1997]. *Hocke*, [1997] identified "wavelike structures" in the upper stratosphere in GPS retrieved temperatures. Since we cannot determine whether these are real or simply noise in the observations, we simply chose not to trust the GPS refractivity observations above 30 km. We therefore assigned a 50% error in observed refractivity above that altitude.

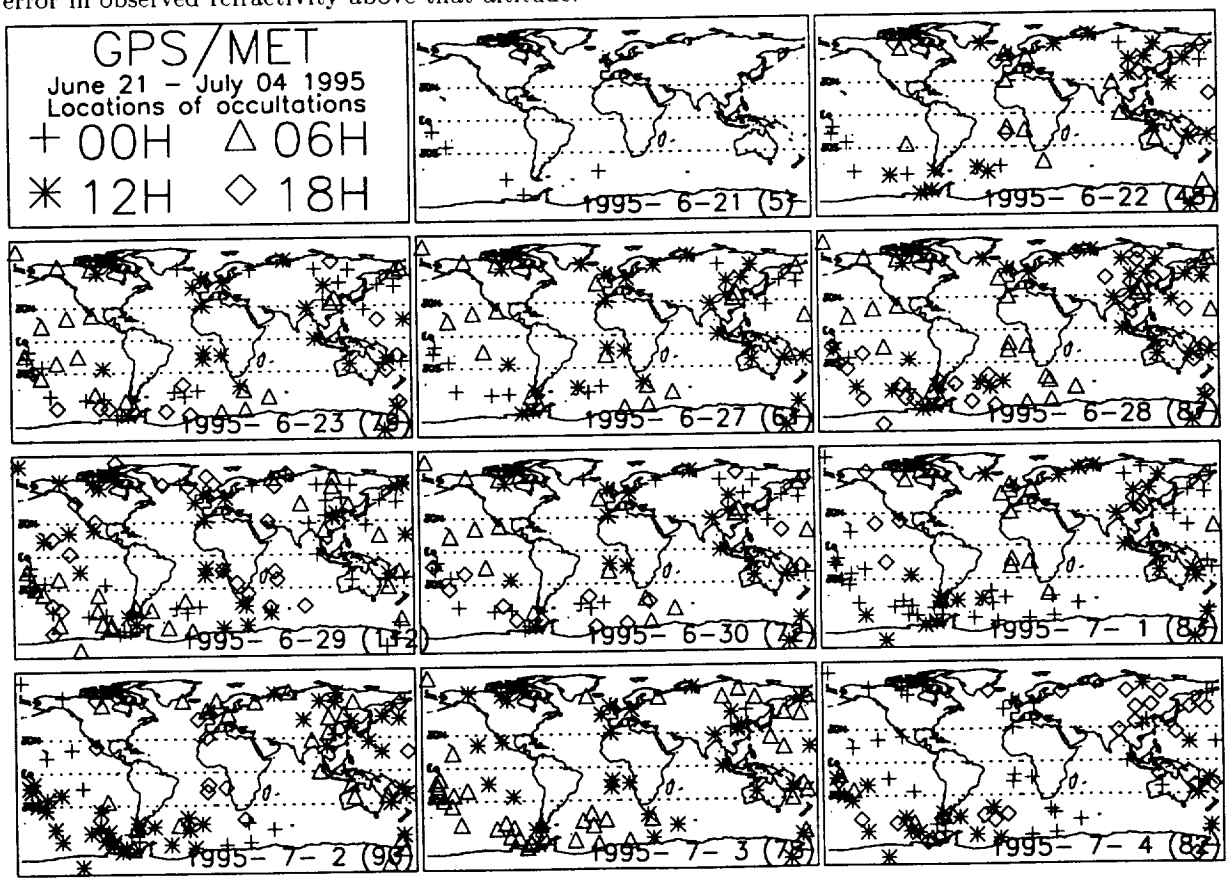

Figure 6. GPS/MET Occultations with no GPS encryption, June-July 1995, processed by JPL. The chart is one map per day and the dates are shown at the bottom of each map, with the number of occultations for the day in parentheses.

5.5. The Observation Operator

The observation operator converts temperature, humidity and pressure profiles into refractivity profiles expressed as a function of altitude. It contains the physics of the measurement and an appropriate space-time interpolation. We assume here that all observations happen at the synoptic time for which our background estimate is valid. The background profile at the observation location is obtained by interpolating bilinearly between the model grid points. It follows that (1) computing refractivity and (2) mapping pressure levels onto altimetric levels are the two main features of this operator.

Instead of performing the analysis on the levels of the forecast, it is possible to work on more levels, for example the levels of the observations. It seems more appropriate to do so in order to obtain analyzed profiles that account for the high resolution features detected by the GPS and that cannot be tracked with a coarse analysis. However, the profiles are to be assimilated in a global circulation model (GCM) and thus must be brought back to a lower vertical resolution, more consistent with the model's dynamics. This is the reason why we chose to work on the levels of our background information. Moreover, the cost of computing on 18~46 levels is much smaller than 60~90 (typical number of GPS refractivity observations for one occultation).

There are two different ways of performing the forward operation : (1) computing refractivity at each model level, then extrapolating refractivity profile expressed in pressure levels into a profile expressed in altimetric levels ; (2) extrapolating model values from each pressure level to the altitudes of the GPS observations, then computing at each point the refractivity value.

Since our goal was to obtain the best profiles for further assimilation, we decided to calculate refractivity first and to interpolate it after. This requires only one interpolation. In addition, calculating refractivity with interpolated values for temperature and water vapor content is likely to generate

complexity in the computation of the Jacobian.

Refractivity values are computed for each model level. For each of these levels, the altimetric altitudes are calculated using a hydrostatic integration. Assuming $P_{sealevel}$ corresponds to 0 meter altitude, the refractivity values are interpolated to the altitudes of the observations using a linear in log of pressure interpolation scheme.

5.6. Linearized Version of the Observation Operator

In (6) we must not only have an observation operator h, but also it's linearized version H. H is the Jacobian or partial derivatives of the observation operator with respect to the various elements of the state vector. We derived an analytical formulation for H. As a check, it was compared with a computation by finite differences as in [*Eyre et al.*, 1993].

The refractivity at one level is found to be sensitive to a variation in temperature and humidity at that level and under that level. This is the result of the integrated altitude calculation using hydrostatic equilibrium. A change in the state vector at a given altitude has no influence on the simulated refractivities located below, but influences the altitudes of the pressure levels above, and hence the refractivity. Figure 7 shows a few columns of the H matrix.

Figure 7

An increase in temperature means a decrease in refractivity at the same level. It has no influence on the calculated refractivities below. The value of the refractivity at each pressure level located above does not change. However, due to the increase in temperature and hydrostatic integration, all the pressure levels above are put higher. This results in shifting upwards the upper part of the refractivity profile, and increasing refractivity for a given altitude.

Increasing humidity increases the local refractivity (the plot is for $-log(q)$). It has no significant influence through the hydrostatic integration.

The sea level pressure has no direct influence on the refractivity values of each model levels. However, it increases the pressure difference between each model level and the sea level, which is the same as increasing the altitudes. The final effect is hence to increase refractivity for a given altitude.

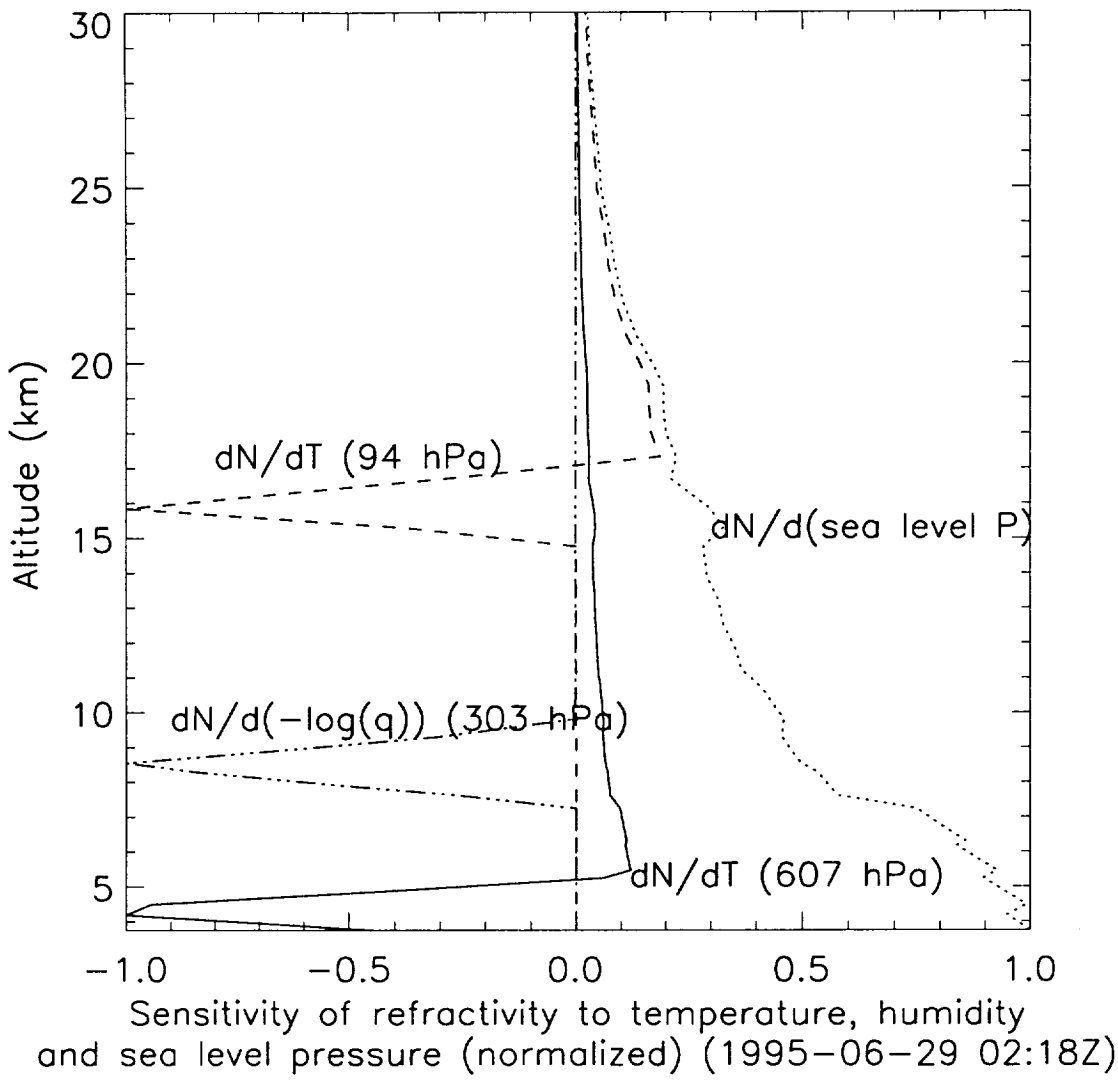

Figure 7. Jacobian for the GPS 1DVAR. Curves for temperature at 607 and 94 hPa, for humidity at 303 hPa, and sea level pressure.

6. Theoretical improvement of GPS data over background information and Monte-Carlo simulation

Knowing the errors contained in the GPS measurements, it is possible to infer the theoretical improvement brought by these data even before having real GPS observations. *Rodgers* [1990] has

proposed linear methods to evaluate the accuracy of a retrieval. They do not require simulated observations, contrary to non-linear methods.

6.1. Linear Analysis

Besides solving the temperature/humidity "ambiguity problem" the 1DVAR approach gives also an appraisal of the quality of the analysis. Under the hypothesis of linearity and Gaussian error distributions, the error-covariance matrix of the analysis P^a is

$$P^a = \left(H^T R^{-1} H + B^{-1}\right)^{-1}, \tag{9}$$

[e.g. *Rodgers,* 1990]. The elements on the diagonal represent the variance of the solution with respect to the 'true state' that we try to estimate. The interpretation of the results given by this method must be taken with caution, because of the hypotheses used: e.g. no bias, no correlation between different types of variables, perfectly estimated background and observation errors.

In the calculations, we assume the same errors in the background for all latitudes. We assume a GPS refractivity vector containing 56 elements, from 1 to 56 km altitude. The associated errors are 2% below 5 km and 0.2% above (up to the top). To gauge the influence of the latitude, we use the same atmospheric profiles as *Joiner and da Silva* [1998].

Figure 8 shows the estimated standard deviation at various levels for both the background and the analysis (see legend as "Linear analysis"), for an atmospheric profile located at 30°. At lower latitude (18°, see figure 9), below 400 hPa, the water vapor content is important enough to play a role *via* the wet term in the refractivity in (4). But at higher latitudes (37° and 63°. see figure 10), the influence of water vapor is less important. The retrieval is therefore not as accurate in deriving fractionnal water vapor content. Concerning the temperature, the analysis has a significantly lower standard deviation than the guess. This result stands for all latitudes.

Figure 8

figure 9

figure 10

6.2. Monte-Carlo Simulation

In order to confirm the previous results and to test the 1DVAR, a fully non-linear Monte-Carlo study is performed. Four experiments were carried out.

In all experiments, 1000 atmospheric profiles are created. A basic atmospheric profile (the "truth") is perturbed. The direction of the perturbations originate from the eigenvectors of the background covariance matrix. In each orthogonal direction, the intensity of the perturbation is obtained multiplying the corresponding square root of the eigenvalue by a random number (normal distribution). Finally, the sum of all the perturbations and the original "true state" give the background estimate.

6.2.1. Observations : No Error Added. For the observations, the refractivity profile is taken as the exact result of the observation operator applied to the true state. No error is added. We ensure that 1000 profiles are enough to generate a distribution with no significant bias as assumed in the theory (e.g. after generation of the population the temperature bias is less than 0.06K). Figure 8 shows the statistical results of the experiment. They are better than what is expected from the linear error analysis which assumed observational errors. We can see that by neglecting the observation errors in an OSSE, we may slightly overestimate the impact of the observations.

6.2.2. Observations : Errors Added. Here, the observed refractivity profiles are perturbed. Errors are added about the exact simulated refractivity obtained from the true state, using the eigenvalues and eigenvectors of the observation error covariance R. Three experiments are made for three different atmospheric profiles, each of them characteristic of a specific latitude (Tropics, Mid-latitude, High-latitude).

Figure 10 and figure 11 show a good agreement with the linear error analysis results. This yields an important point : the 1DVAR works correctly with simulated data (total of 3000 analyses, all converged).

figure 11

Under the above hypotheses, refractivity data are expected to bring some improvement for temperature at all latitudes. For the humidity, the best improvements may happen in regions with a relatively high amount of water vapor (i.e. Tropics, mid to lower troposphere). *Palmer et al.* [2000]

and *Healy et al.* [2000] have obtained similar results.

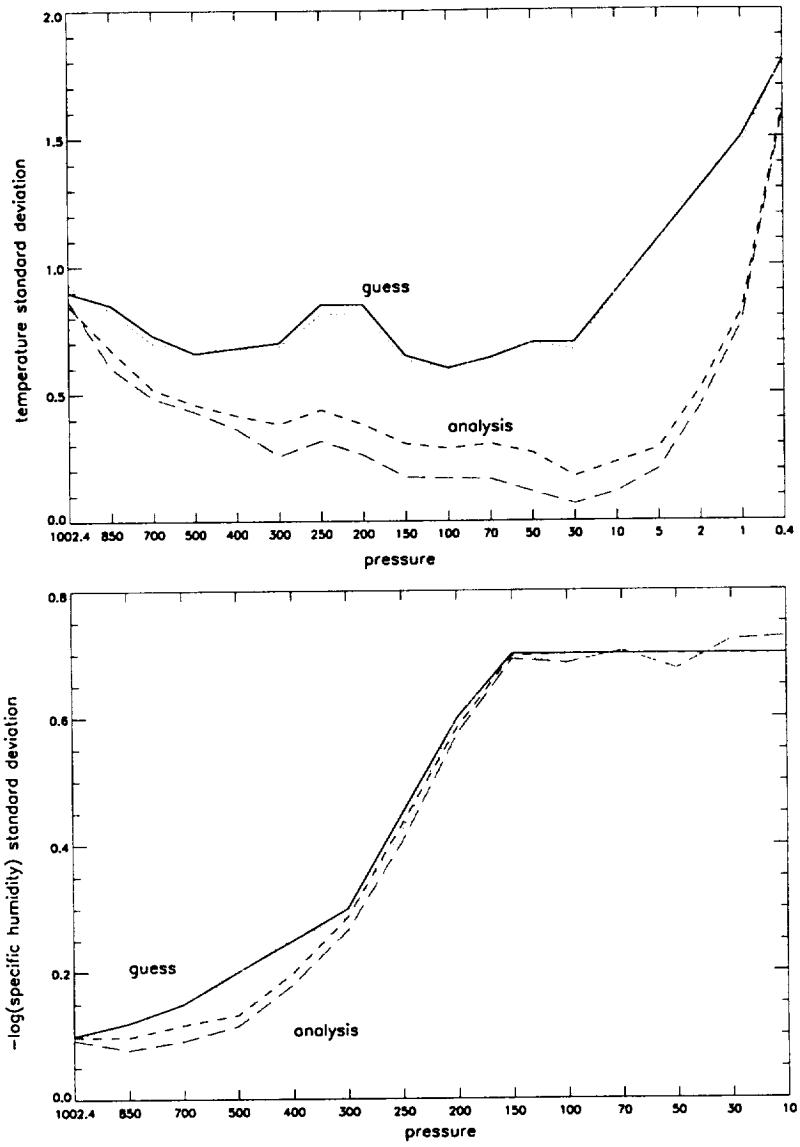

Figure 8. Standard deviation of : *top* : temperature ; *bottom* : log specific humidity. Linear analysis assumes noise in the GPS observations: results are in plain line for the guess estimate and short dashes for the analysis. Monte-Carlo simulation is performed with no noise in the observations: the curves are dotted line for the guess and long dashes for the analysis.

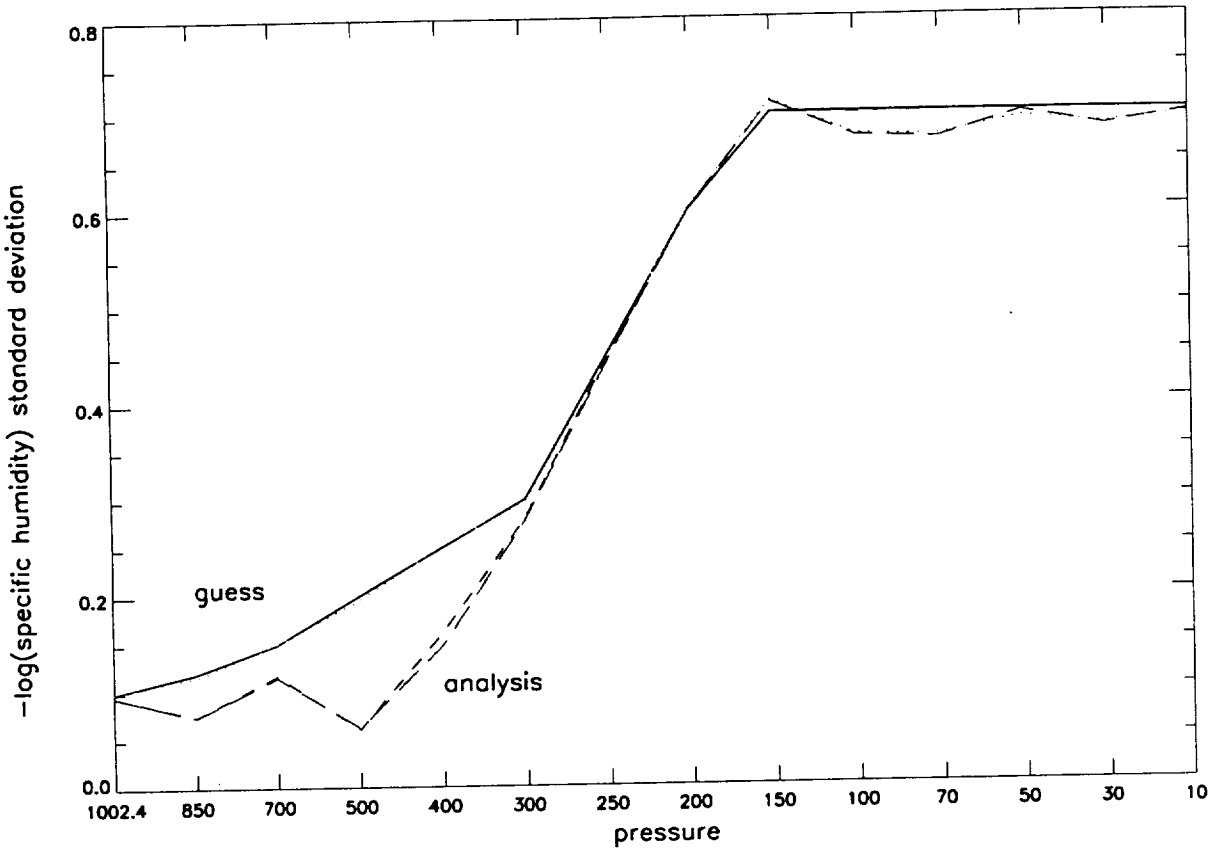

Figure 9. Standard deviation of log specific humidity, latitude 18°. Curves are as described in figure 8 with the difference that noise is added to the observations in the Monte-Carlo simulation.

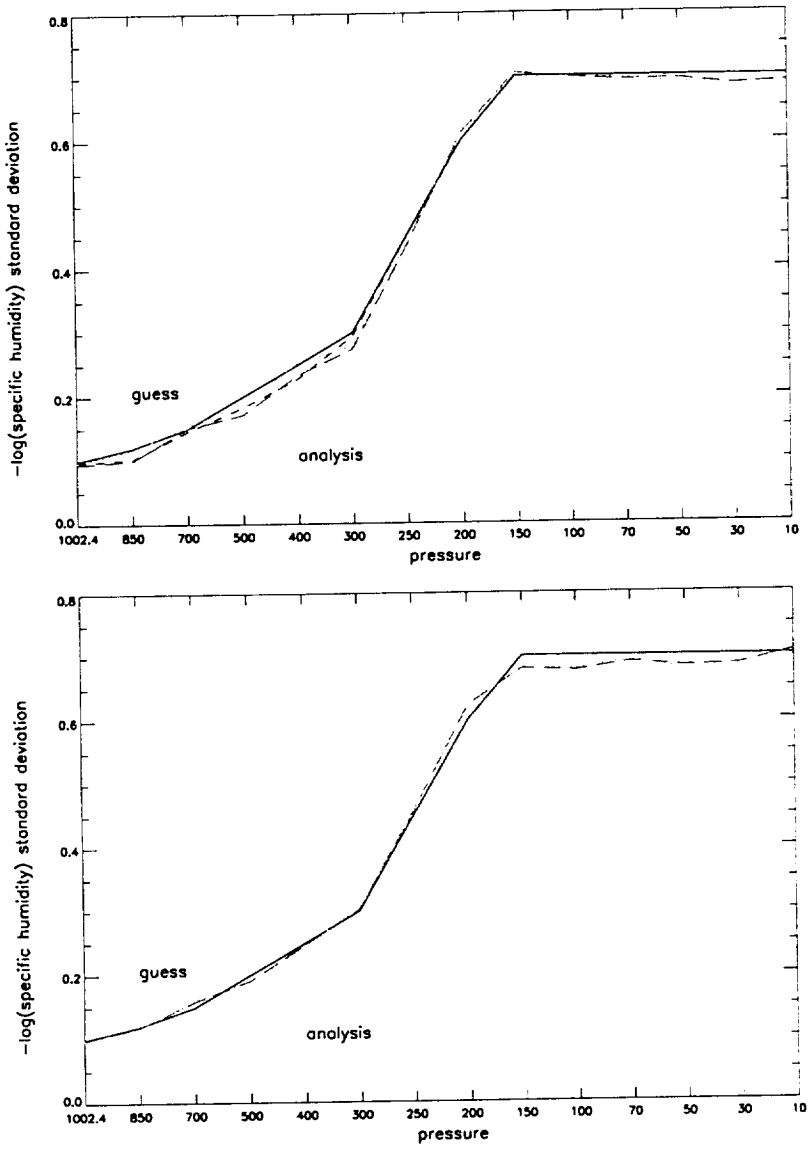

Figure 10. Same as figure 9, but for latitudes 37° (*top*) and 63° (*bottom*).

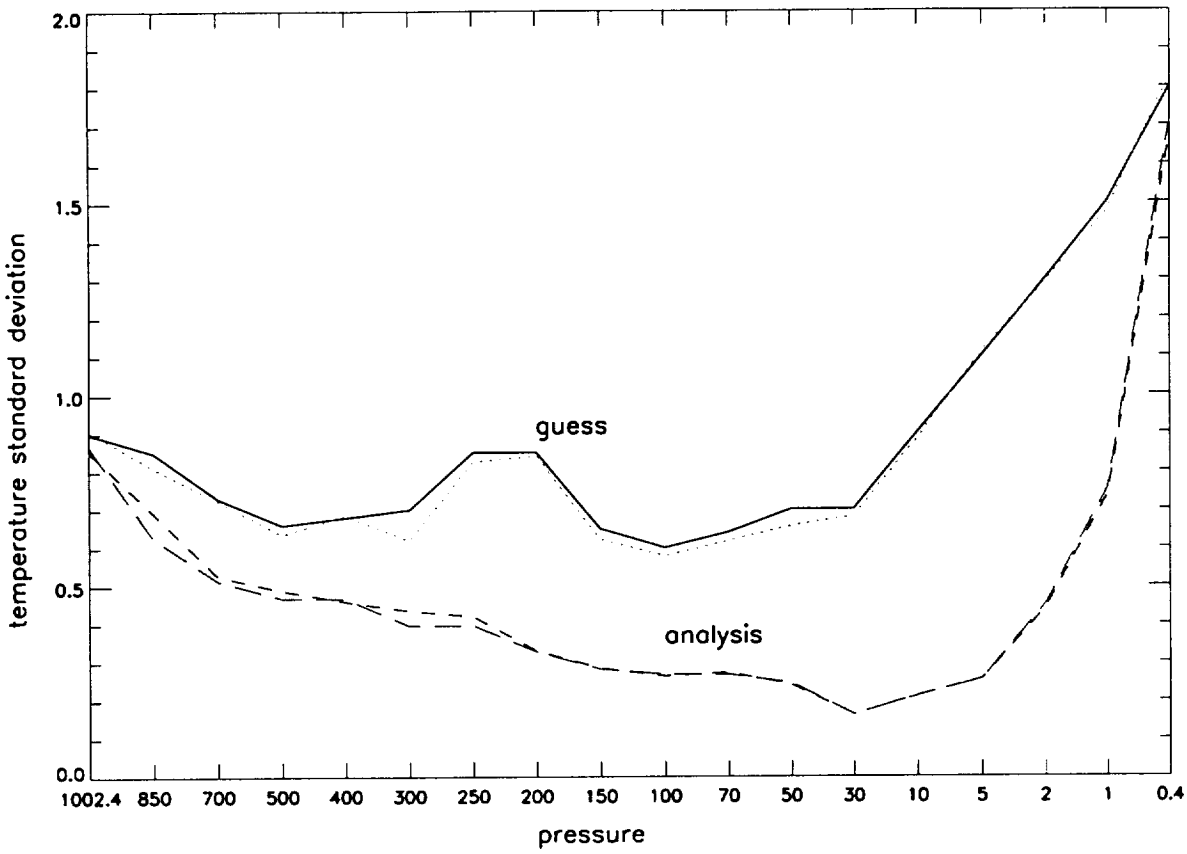

Figure 11. Same as figure 9, latitude 18°, but for the temperature.

6.3. Averaging Kernels

The repartition of information brought by the GPS 1DVAR can be made by looking at the averaging kernels [*Rodgers*, 1990]. They are computed the following way: (1) for the temperature, a 1 K impulse is added in the state vector at one level (2) the observation operator is applied to that state of atmosphere to obtain a refractivity profile which contains effectively the 1 K impulse (3) we perform a 1DVAR analysis using for the background the unperturbed state vector (4) the difference between the retrieved temperature and the original state vector gives the response of the system. This is repeated for each level of the guess estimate. If the observations contained perfect information content and no weight was given to the background, the response would be equal to the original unit impulse, and focused at the same level only. Figure 12 testifies that the 1DVAR analysis keeps the relatively high

Figure 12

vertical resolution of the observations.

In the given example, the observations start around 5 km altitude. The state vector is shortened so that only levels located above that altitude are modified by the analysis. Consequently, the response of the system to a 1K impulse located anywhere below that level is zero.

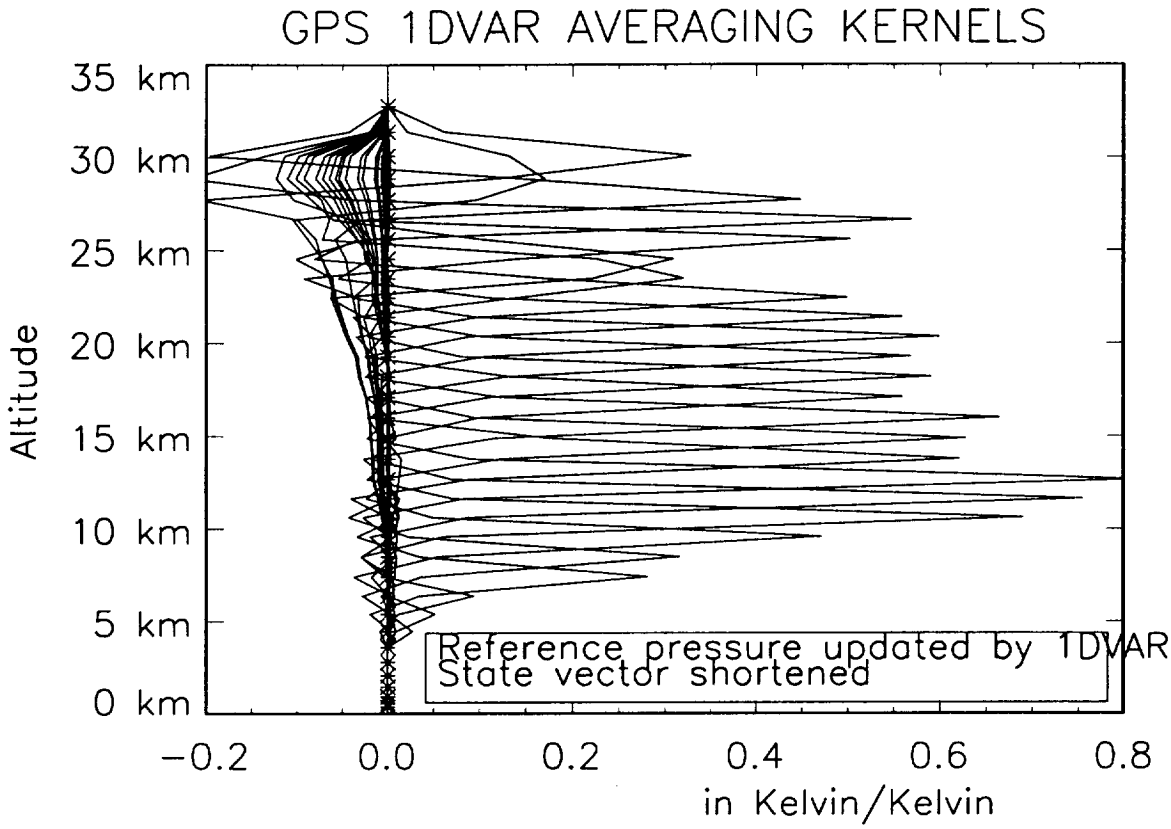

Figure 12. Temperature averaging kernels for the GPS 1DVAR.

7. Sensitivity of the retrievals to various parameters

7.1. Sensitivity to the Number of Levels in the Guess

We will now focus on a single occultation which occurred on June 21st 1995, at 00:03UTC, at (10°S, 168°W). Three relevant temperature profiles are discussed here : the first-guess estimate (6-hour forecast of the GEOS model), the analysis obtained through the 1DVAR retrieval, and the direct

retrieval (assuming a humidity profile). The latter depicts how the "raw" refractivity data see the atmosphere. Here we assume that the temperature/humidity ambiguity problem will not lead to a misinterpretation of the data. The refractivity data start at 6600 m for this observation. Therefore, the risk of misinterpretation is limited, even though the occultation occurred in the Tropics. For the 1DVAR analysis, the error in refractivity is taken as 2.% up to 5 km, and 0.2% above, with no inter-level correlation.

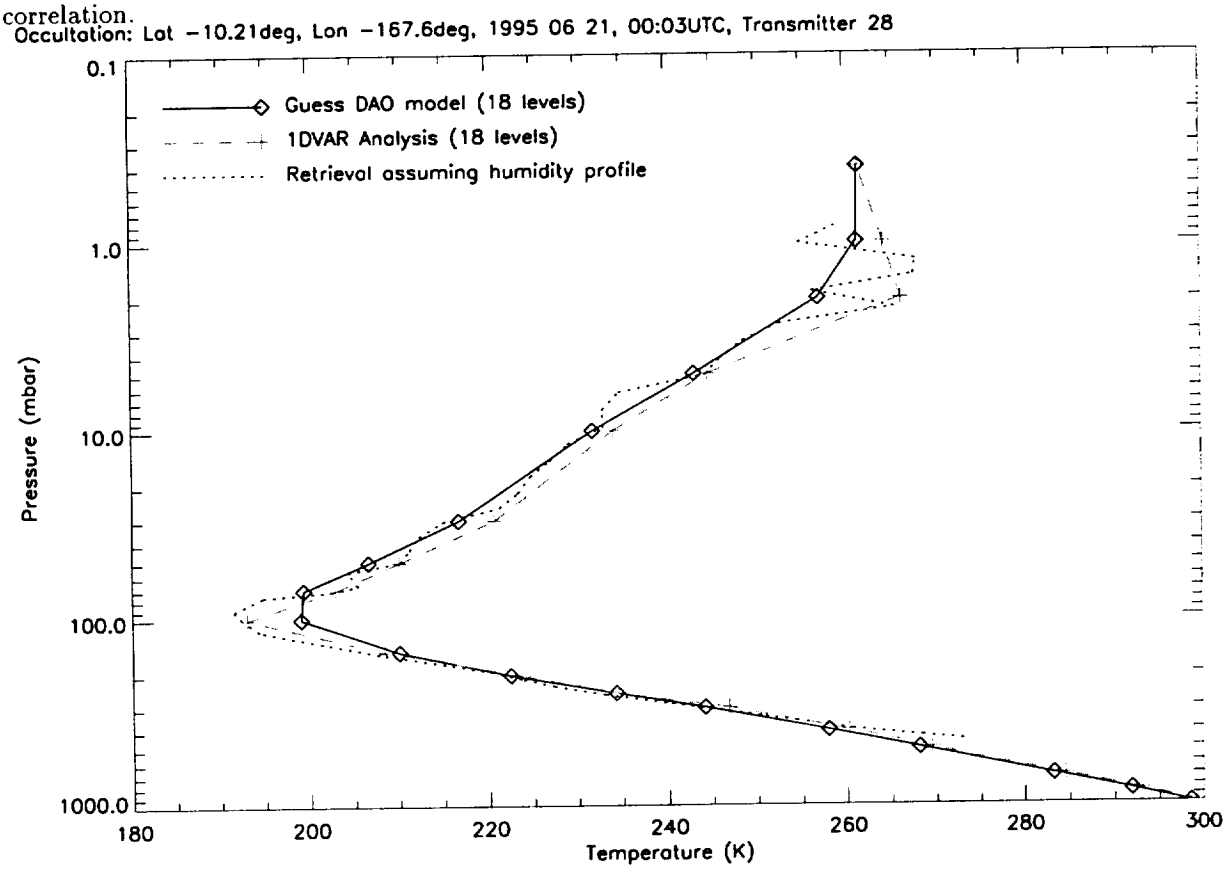

Figure 13. Temperature profile, 1DVAR analysis performed on 18 levels.

Figure 13

7.1.1. Analysis on 18 levels. Figure 13 shows the result of an analysis performed with background information on 18 levels. These levels are the available archived levels. The 1DVAR works on the same levels as those of the background and hence the retrievals are also on 18 levels.

The fine resolution of the GPS measurements as inferred by the direct retrieval appears to produce some high frequency structure in the stratosphere. The 1DVAR tries to simulate this structure, as the

observation errors are relatively small as compared with the projected background errors. However, due to the coarse resolution of the state vector (based on the 18 levels of the guess), the analysis cannot fully resolve these structures.

The background used to perform the error analysis study and Monte-Carlo simulation was on 18 levels. These studies did not take into consideration any inconsistency between the resolution of the observing system and the guess. However, the data have a finer resolution so that a coarse-resolution 1DVAR cannot fully resolve the structure.

7.1.2. Analysis on 46 levels. Another first-guess estimate is used here. This guess consists of 46 σ levels, with a top at 0.1 hPa. The σ levels are converted to pressure. Figure 14 shows the result of the analysis of the same refractivity profile on 46 levels. We can see some "waves" in the analysis at this resolution. We also see a large increment at the top of the profile. Note that the structure at the tropopause is now much better resolved than before at low resolution. This shows the need to analyze the GPS at a higher resolution than the GEOS-Strat analysis if the full impact is to be realized. As explained in section 5.4, we will subsequently increase the errors of GPS observations in the analysis above 30 km.

Figure 14

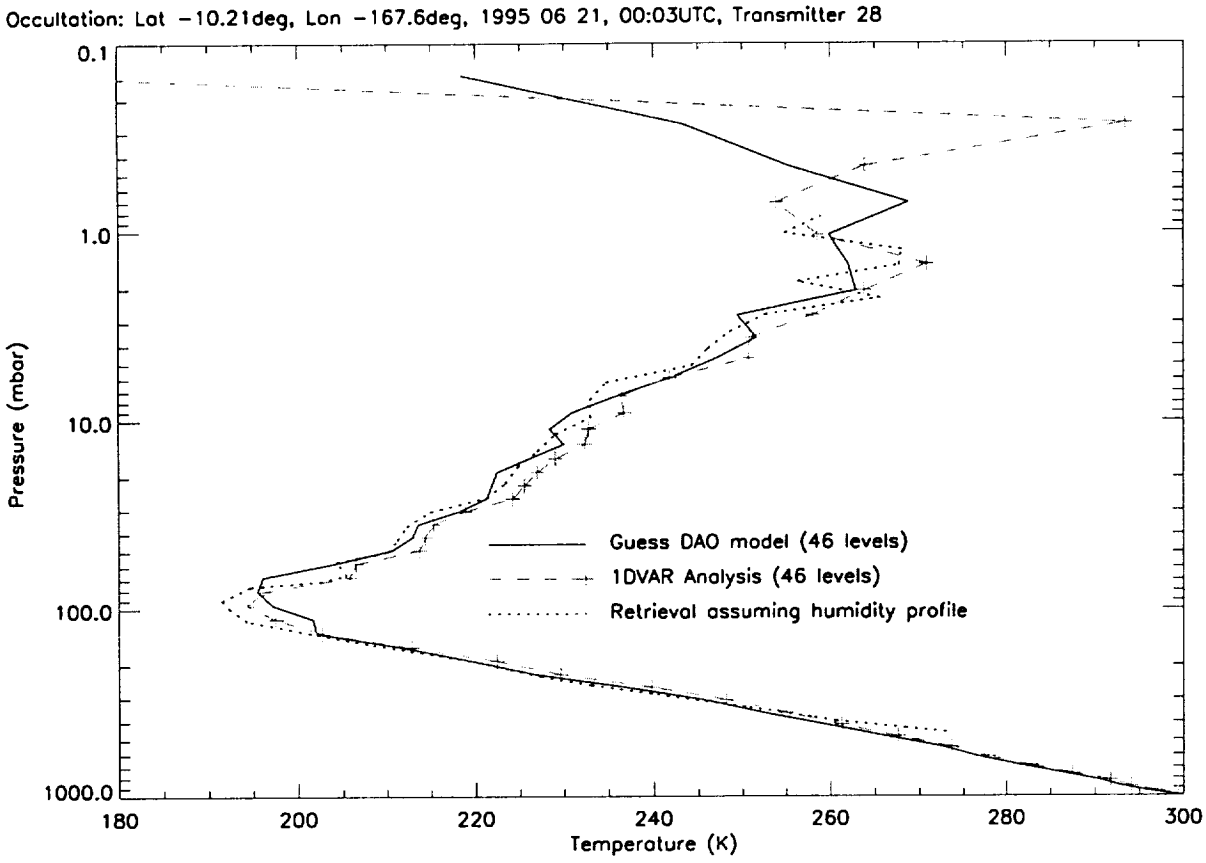

Figure 14. Temperature profile, 1DVAR analysis performed on 46 σ levels.

7.2. Sensitivity to the gravitational force

One unexpected result is the sensitivity of the analysis to the gravitational constant used in the analysis. We used two formulations for g. (1) g=9.80665 m·s^{-2} (2) g=$g(z)$ [*Healy.* 1998]. The second gave better results by comparison with radiosondes.

Depending on the approximation used for the definition of g, differences of order 1K can appear. This sensitivity to the gravitational constant is specific to GPS measurements. It arises from the conversion from pressure (the levels of the analysis) to altitude (the levels of the observations).

7.3. Sensitivity to the Surface Pressure

The surface pressure also affects the computation of the altitudes. It is used as a reference to integrate the hydrostatic relationship.

The analysis increment is defined as the difference between the 1DVAR retrieval and the initial background. Figure 15 shows two different increments. The first one is calculated with a fixed reference pressure, i.e. the same as in the background estimate. In the second implementation, the reference pressure becomes part of the state vector and hence can be updated. Overall, radiosonde comparison statistics are improved by this modification. When the reference pressure can be updated, the whole refractivity profile can be moved upwards or downwards. When it is not possible for the system to do that, its only alternative is to increase or decrease the temperature on several layers so that the layers can get thicker or thinner.

Figure 15

Adding this degree of freedom enables the 1DVAR to account for any inconsistencies that may exist between the guess and the observations concerning the definition of the sea level. It may also limit the errors due to the interpolation of the sea level pressure from the background fields.

To illustrate this, taking the example of occultation 1995-06-28 at 09:31Z, the computed altitude of the level 10hPa is moved from 31,160 to 31.290 meters (after minimization) when the sea level pressure (SLP) cannot be moved by the analysis (i.e. the difference is created by the adjustment made on the temperatures). When the SLP is included in the state vector, the temperature increments are smaller, but the computed altitude is about the same as before at 31,280 meters.

8. Comparisons with Radiosondes

8.1. Collocation

The statistics shown here are computed by collocating results of GPS 1DVAR analyses with nearby radiosondes (RS). The criteria for collocation are +/- 3 hours, less than 280 km. The temperature (humidity) direct retrievals obtained using an estimate of humidity (temperature) from the European

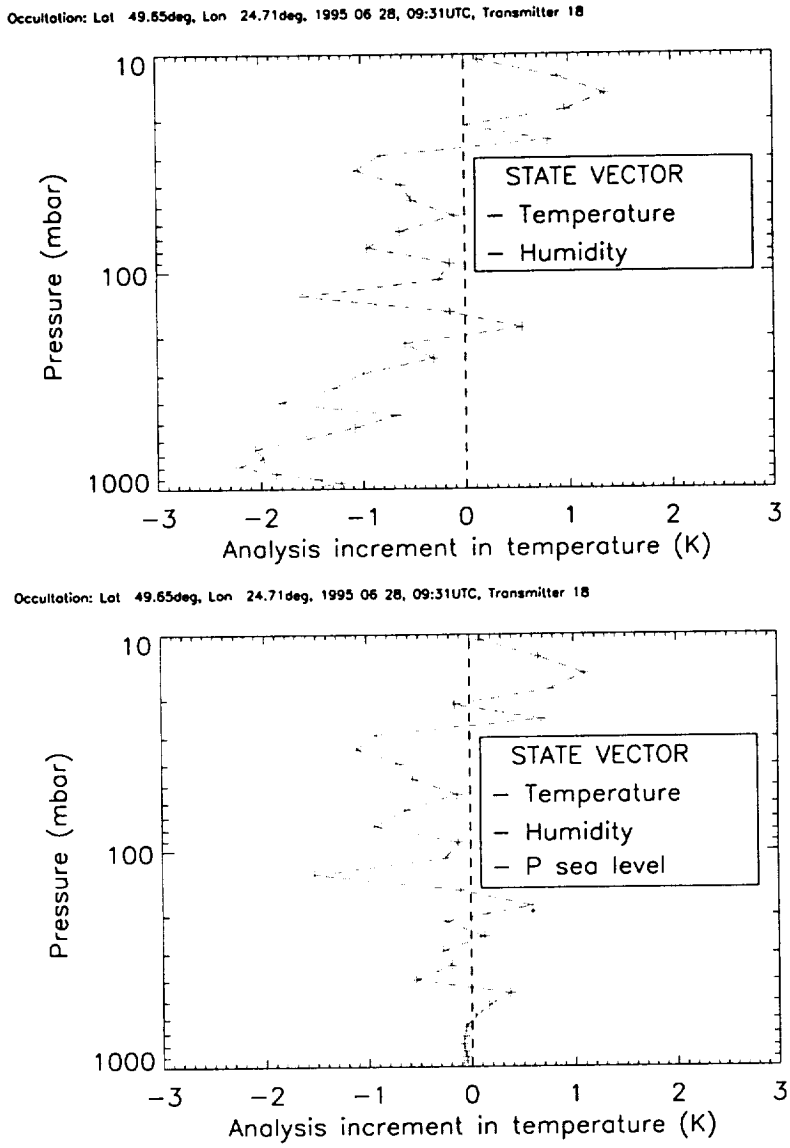

Figure 15. Temperature analysis increment. *Above* : sea level pressure of the background assumed as correct - *Below* : sea level pressure included in the state vector

Centre for Medium-Range Weather Forecasts (ECMWF) analyses are also shown [*Kursinski et al.*, 1997].

Among the 797 GPS occultations, about 150 match the collocation criteria. Results are not shown for the southern hemisphere (beyond 30°S) because of a very small number of comparisons. Only one 1DVAR minimization process did not converge. As a background check, collocations with discrepancies more than 5 K between background and RS are removed from the statistics. It is necessary to apply some quality control to the RS and the direct retrievals. Therefore, we also remove discrepancies more than 5 K between the RS and the direct retrieval. No quality control is performed on the 1DVAR analyses themselves.

The same policy is applied for humidity, expressed in terms of difference of specific humidity (in percent). All differences, background minus RS or RS minus direct retrieval, greater than 100% are removed.

8.2. Temperature

Figure 16 shows a single temperature profile which exhibits the advantages of combining model estimates with real observations. (1) Both direct retrieval and 1DVAR analysis are able to resolve the tropopause better than the GEOS assimilation. The background has a warm bias at the tropopause of about 5K. (2) In the lower layers, the analysis follows the background, whereas the direct retrieval notably diverges from the RS.

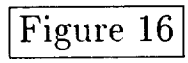

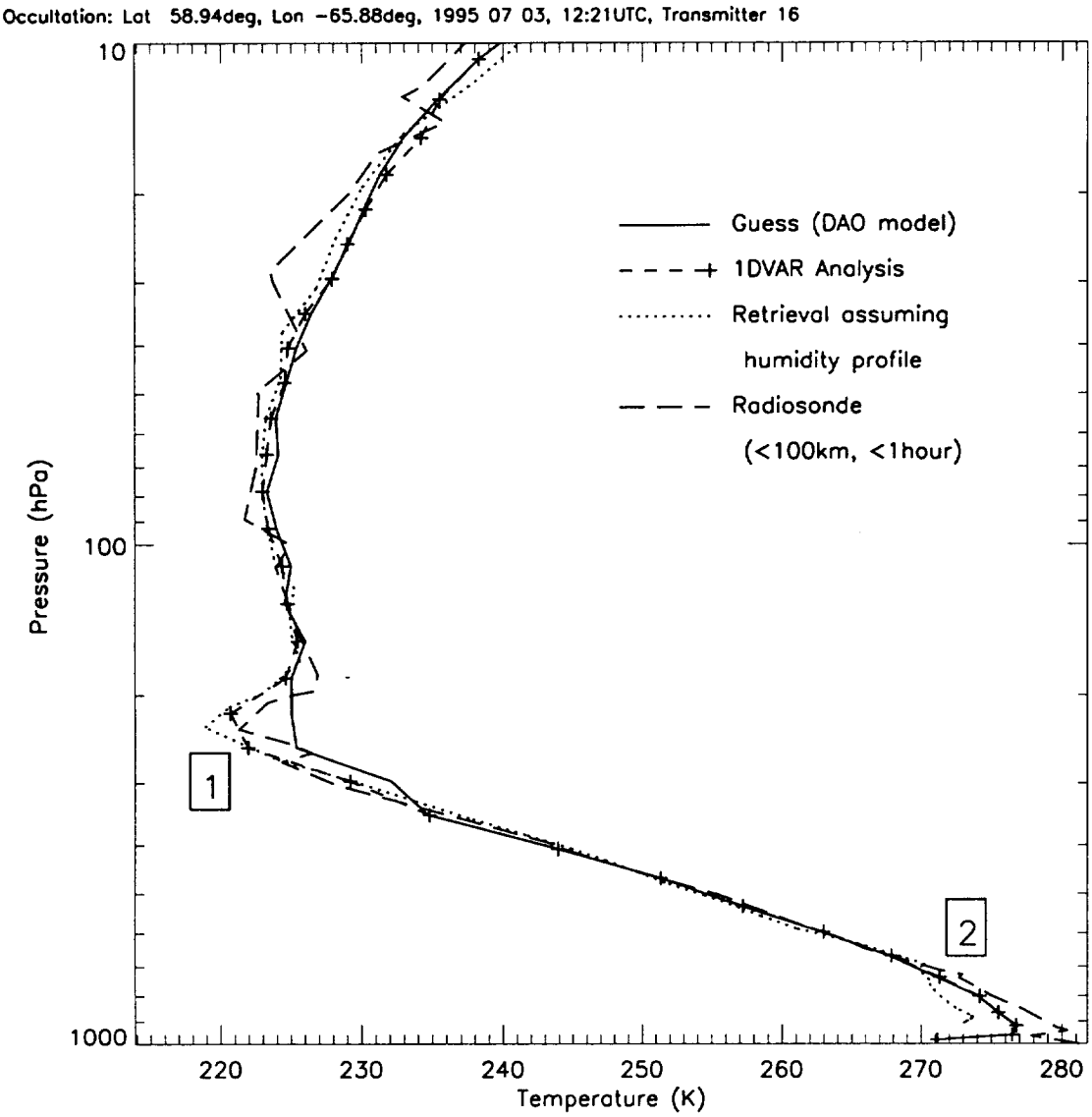

Figure 16. Temperature profile showing the advantages of using a variational approach with GPS data.

Figure 17 presents the biases and root-mean square (rms) difference from collocated radiosondes for temperature in the northern hemisphere (above 30°N). The chart also indicates (to the right) the number of data used to calculate each point. That number decreases towards the surface because most of the occultations did not reach the surface. The balloon bursts above the tropopause explain the decreasing number of comparisons in the stratosphere.

Figure 17

A significant temperature bias present in the background data at the tropopause is removed by the

1DVAR analysis, between 250 and 100 hPa. The standard deviations are significantly reduced above. Below 500 hPa, a slight degradation can be detected. Overall, the rms of the GPS 1DVAR is reduced as compared with the background at most altitudes.

Similar results are obtained in the Tropics. Figure 18 shows the temperature bias in the tropics (between 30°S and 30°N). Around 100 hPa, the GPS 1DVAR reduces a bias even more significant than in the northern region. Figure 19 demonstrates a net reduction of the rms of about 1.0K at the tropopause.

Figure 18

Figure 19

Figure 20 represents the increments, i.e. the difference between 1DVAR retrieved temperature and the initial value given by the GEOS model. They are largest at the tropopause.

Figure 20

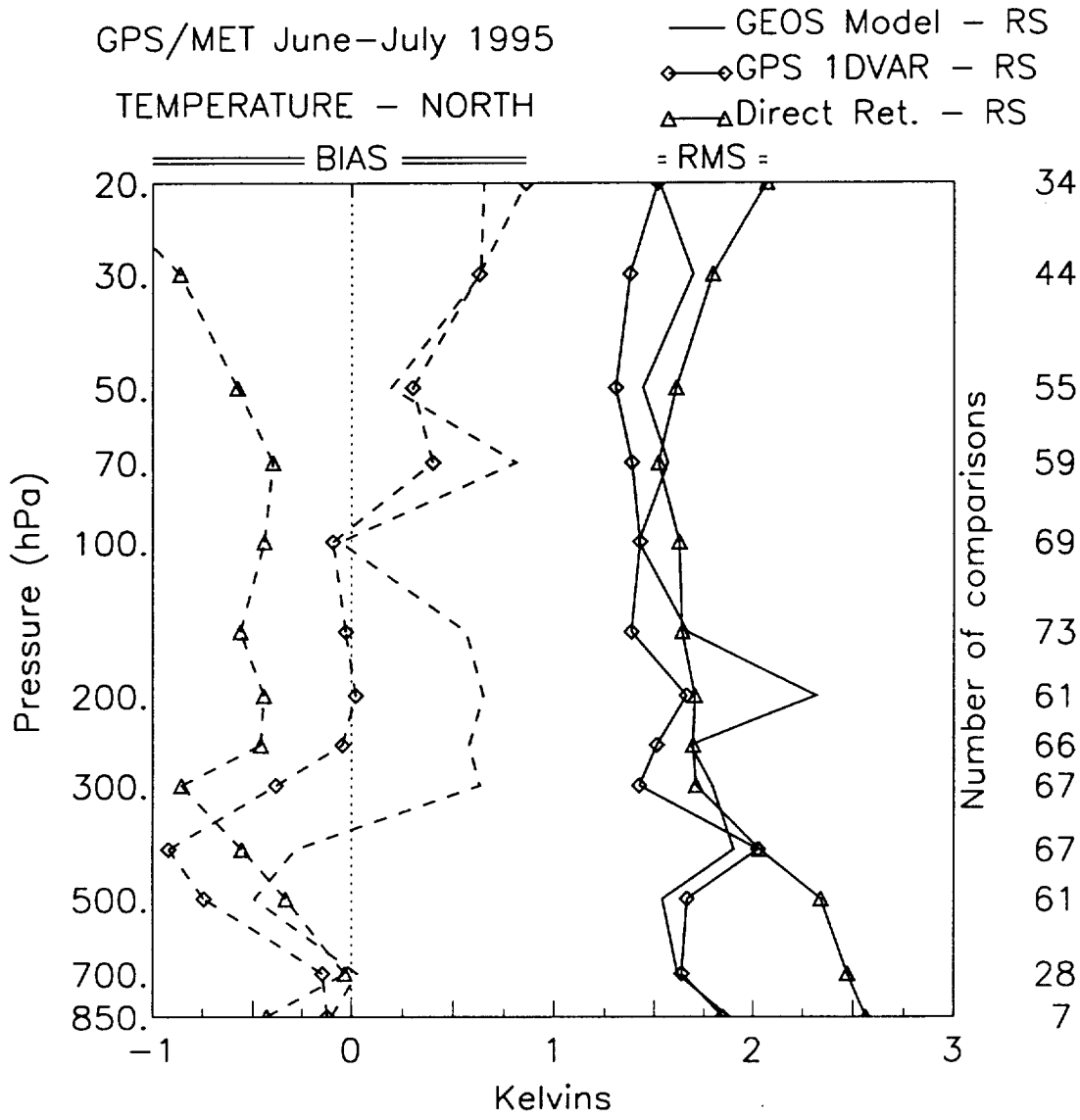

Figure 17. Northern hemisphere, comparisons with radiosondes temperatures (+/- 3 hours, less than 280 km) for the GPS 1DVAR, the background and the direct retrieval. Curves show bias and rms.

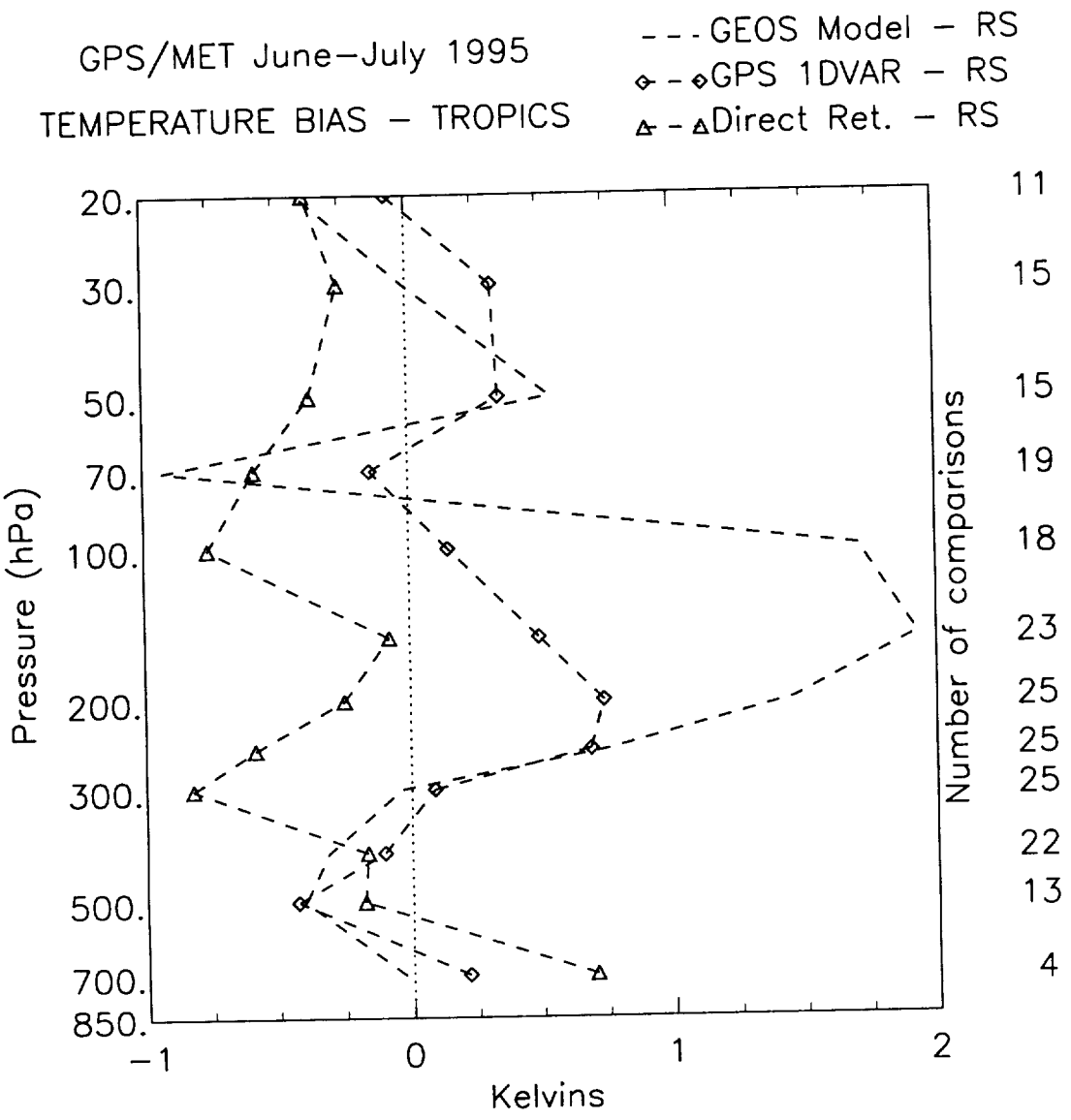

Figure 18. Tropics, bias in temperature determined by comparison with radiosondes.

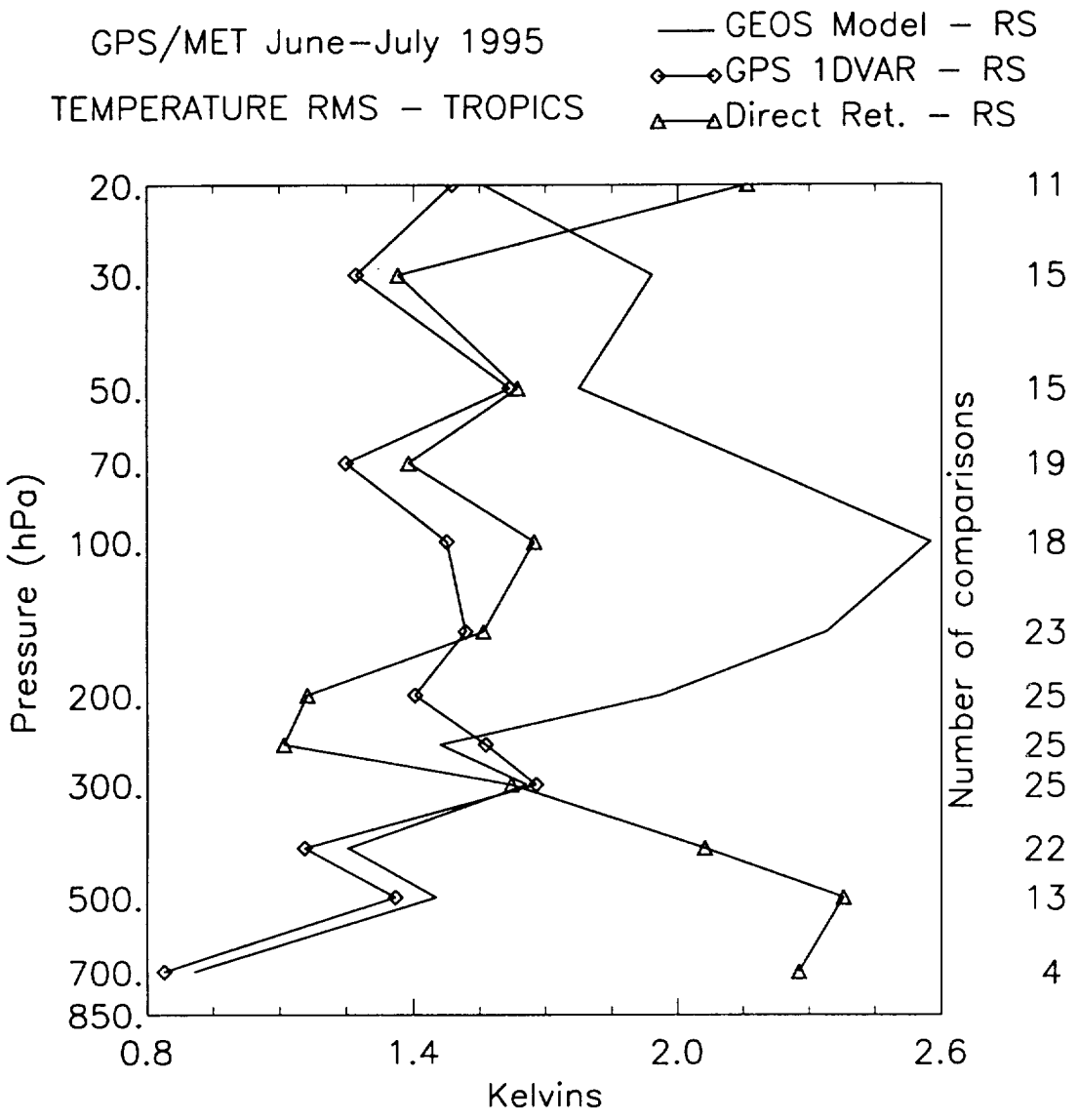

Figure 19. Same as figure 18, but for the temperature rms.

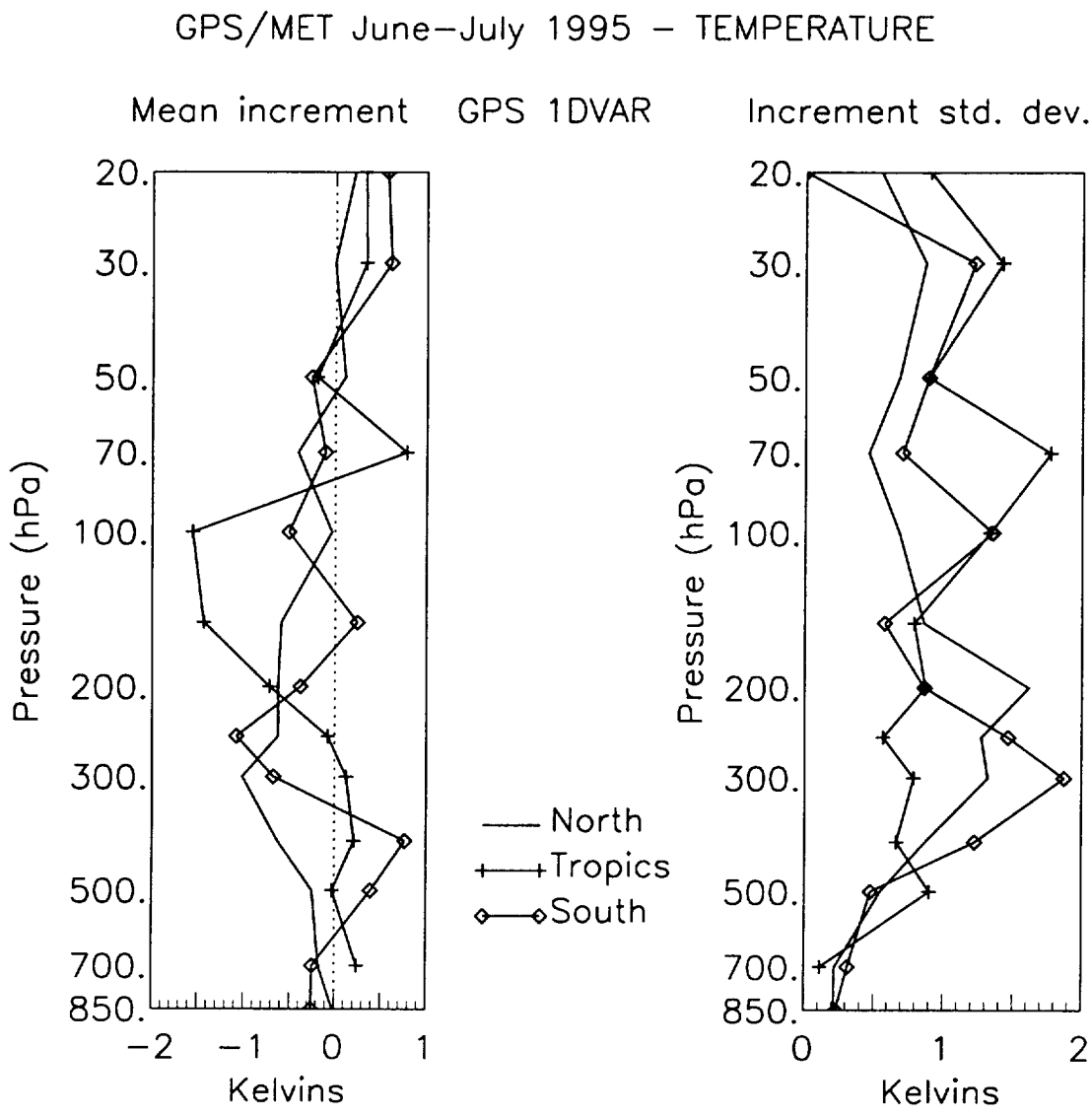

Figure 20. GPS 1DVAR temperature increments.

8.3. Humidity

Many radiosondes we used either did not report the humidity, or the reported humidity was different from the GEOS background by more than 100%. It is known that humidity present smaller scale features than temperature. There are also known problems with RS humidity measurements [*Soden et al.*, 1996]. The collocation criteria chosen may be responsible for many of the discrepancies.

This results in a small number of comparisons. We were not able to find a sufficient number of radiosondes presenting a reasonable difference with the background in the tropics. For this reason, only the northern hemisphere results are presented.

Figure 21 shows bias and rms with respect to collocated RS. Only the 400 hPa level shows an improvement over the background. Some degradation of the 1DVAR as compared with the background is shown at other levels.

Figure 21

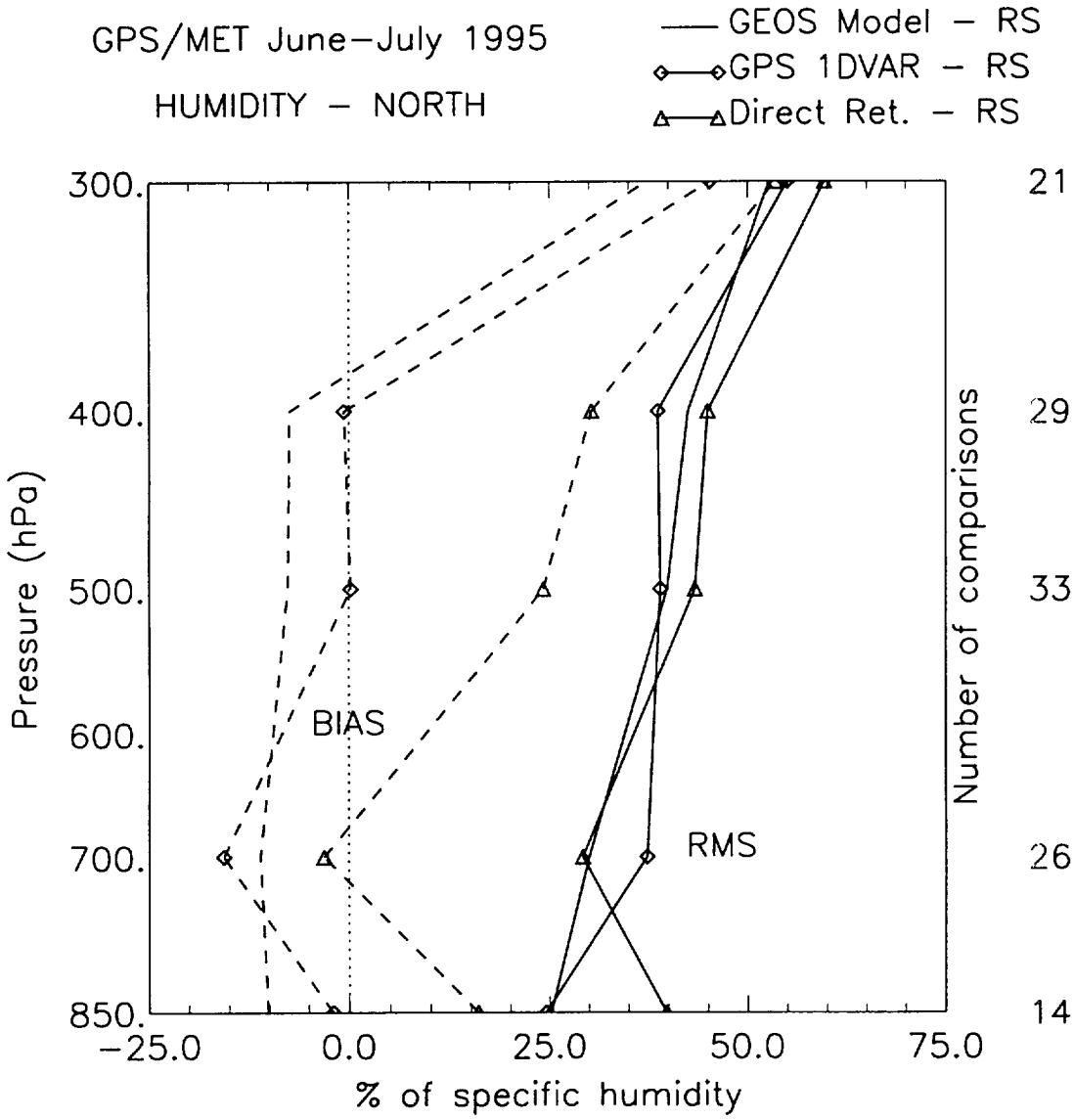

Figure 21. Northern hemisphere, comparisons with radiosondes humidity. Curves show bias and rms.

8.4. Observation residuals

Residuals are defined as the difference between the observation and the simulated refractivity calculated from the model background. Since refractivity spans values of several orders of magnitude, we are looking at it in terms of percent of observed refractivity.

The refractivity varies locally primarily with the inverse of temperature. The fact that the background has a warm bias at the tropopause implies a local negative bias in refractivity as compared to the observations. However, since the above altitudes are computed using the temperature at the levels below, all the refractivity values above don't move. However, the profile of geometric altitudes corresponding to the same pressures is shifted upwards. This results in an increasing positive refractivity bias (see figure 22).

figure 22

In the tropics (figure 23), the negative bias due to the missed tropopause is located higher, around 15 km. Below 5 km, the refractivity differences grow significantly, indicating that (1) phenomena are not simulated correctly by our observation operator and/or (2) there are important errors in the measurements. Horizontal gradients and multipath may appear in either category, depending on the way the analysis is made (i.e. 1D or 3D, refractivity or bending angle, geometrical optics or Fresnel inversion).

figure 23

In the 1DVAR theory, we assumed that both observations and the background are not biased. Clearly they are biased. An interesting point is that even with a bias, the 1DVAR removes some of that bias : the curve for the bias of the 1DVAR refractivity residual is close to zero. However, if we look carefully, some bias remains in the residuals. This is most apparent near the tropopause in the tropics where the background bias was the strongest.

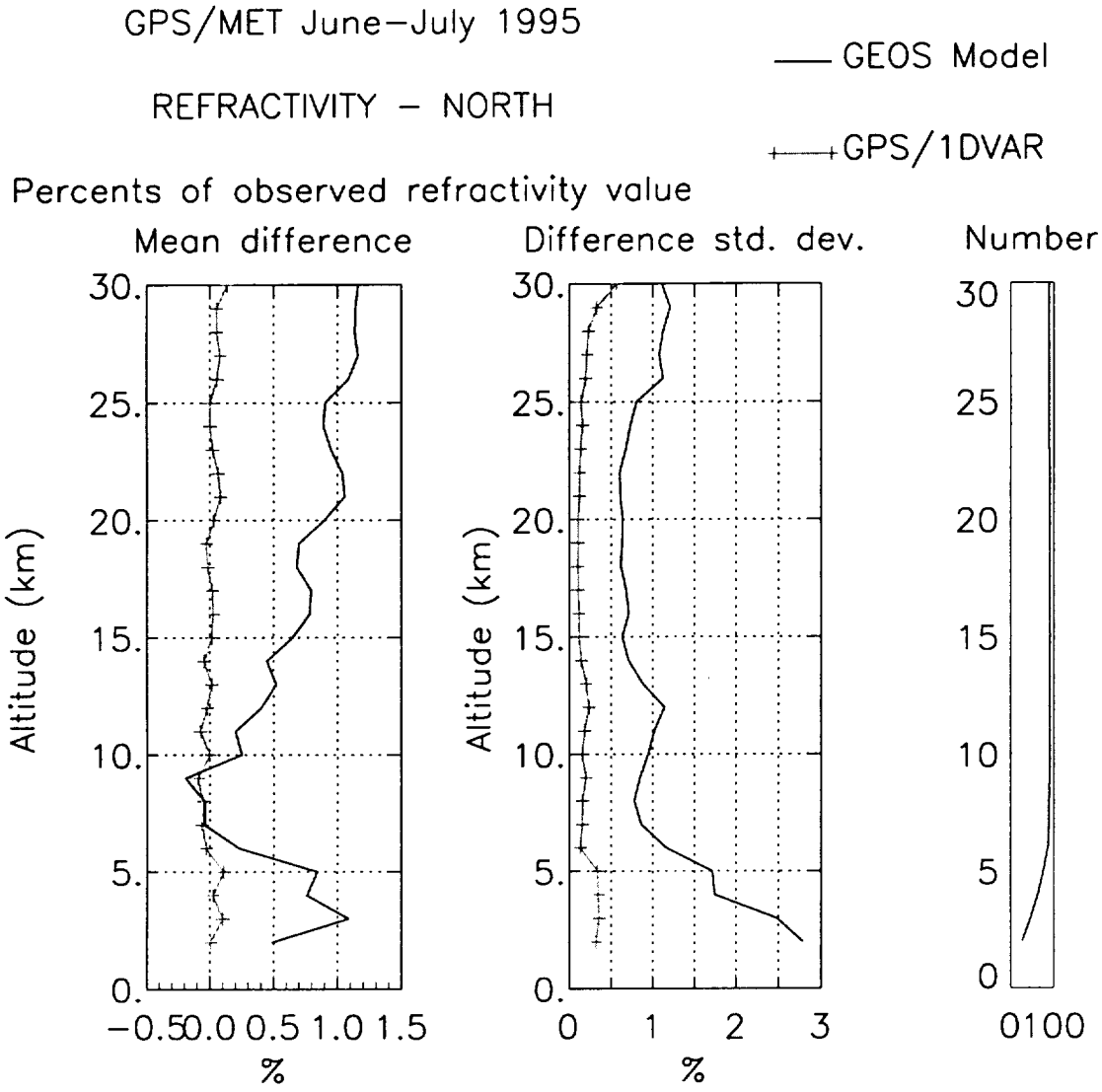

Figure 22. Difference between observed refractivity and simulated refractivity (from the GEOS background), in percents of the observed refractivity, in the northern hemisphere.

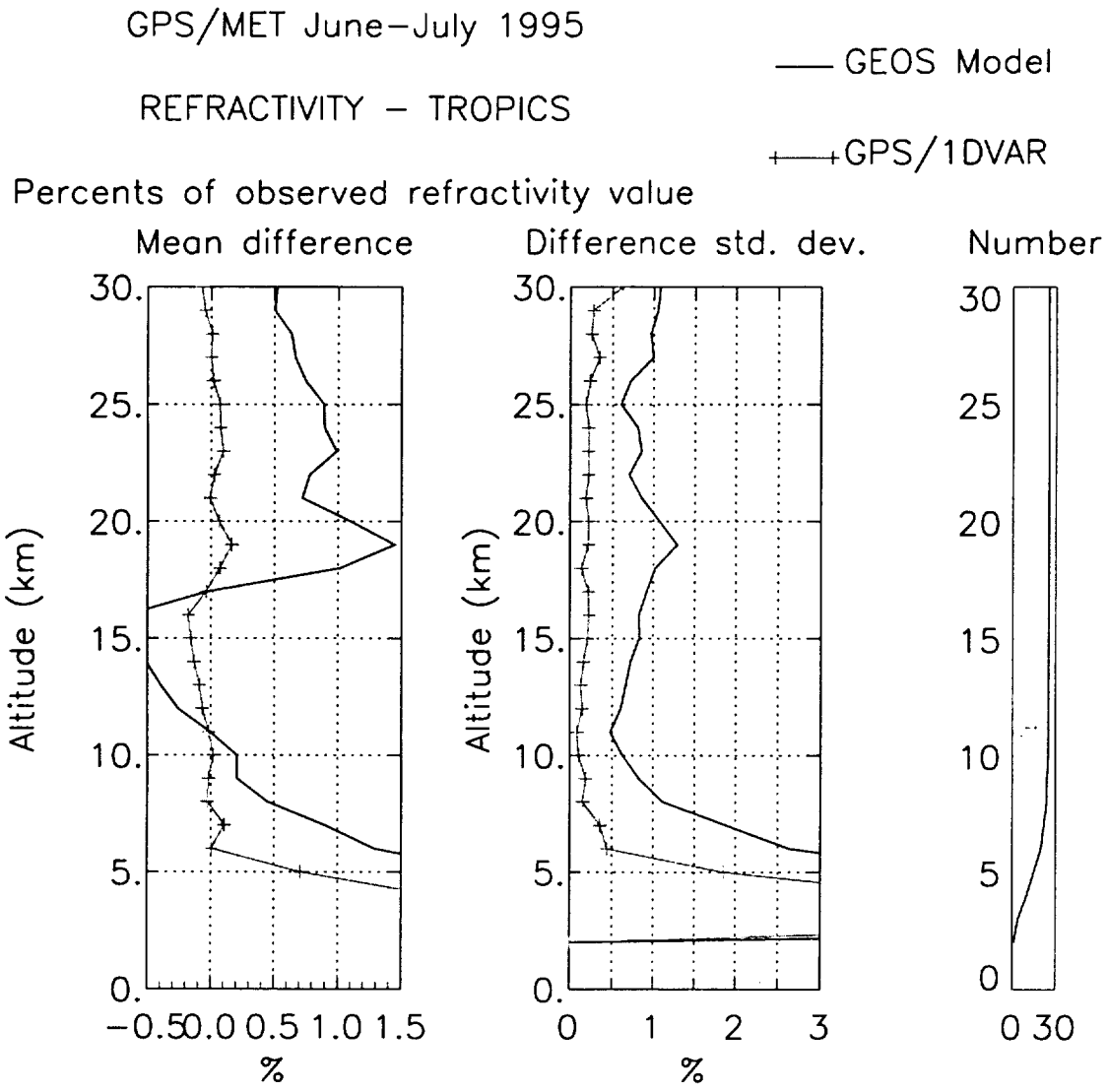

Figure 23. Same as figure 22 (observation residuals), but for the tropics.

9. Conclusions and Future Directions

An overview of the various techniques possible to assimilate GPS data has been presented. We implemented a 1DVAR analysis of refractivity. This presents a good trade-off between computational cost and accuracy. The one-dimensional observation operator is efficient and accurate. Temperature improvements are both expected and observed with GPS/MET data. We saw improvement at some

altitudes in the analysis of humidity with GPS data, but this was accompanied with some degradation at other altitudes.

There are assumptions made when deriving refractivity from bending angles (i.e. local spherical symmetry). Even with this assumption, we have shown that significant improvement in temperature can be obtained by combining GPS observations with an accurate background. However, the limited impact in regions with high water vapor amounts (i.e. below 500 hPa), the strong discrepancy between simulated and observed refractivities and the unexpected sensitivity of the retrievals to the formulation of the gravitational constant testify that some phenomena still need to be studied with care before making any statement related to global trends or impact on NWP based on GPS observations.

After showing a positive impact on the analysis, the next step to demonstrate the usefulness of GPS in weather prediction is to run an impact experiment. The small amount of data collected daily with GPS/MET currently limits the significance of such an experiment, regardless of the quality of the data. More GPS data with improved receivers are expected in the future. They will give an opportunity for more global and case studies.

References

Atlas, R., Atmospheric observations and experiments to assess their usefulness in data assimilation, *J. of the Meteor. Soc. of Japan, 75*, 111-130, 1997.

Bean, B. R., and E. J. Dutton, *Radio Meteorology*, Dover Publications, New York, USA, 1968.

Bevis, M., S. Businger, T. A. Herring. C. Rocken, R. A. Anthes, and R. H. Ware, GPS meteorology: remote sensing of atmospheric water vapor using the global positioning system, *J. Geophys. Res., 97*, 15,787-15,801, 1992.

Bloom, S. C., L. L. Takacs, A. M. da Silva, and D. Ledvina, Data assimilation using incremental analysis updates, *Mon. Weather Rev., 124*, 1256-1271, 1996.

Doerflinger, E., Météorologie/GPS estimation du contenu atmosphérique en vapeur d'eau integré à l'aide de mesures GPS au sol, *Tech. Rep. 19*, 31 pp., Météo-France CNRM/GMEI, Toulouse, France, 1998.

Elgered, G., J. M. Johansson, B. O. Rönnäng, and J. L. Davis, Measuring regional atmospheric water vapor using the swedish permanent GPS network, *Geophys. Res. Lett., 24*, 2663-2666, 1997.

Eyre, J. R., Assimilation of radio occultation measurements into a numerical weather prediction system, *Tech. Memo. 199*, ECMWF, Reading, UK, 1994.

Eyre, J. R., G. A. Kelly, A. P. McNally, E. Andersson, and A. Persson, Assimilation of TOVS radiance information through one-dimensional variational analysis, *Q. J. R. Meteorol. Soc., 119*, 1427-1463, 1993.

Gorbunov, M. E., and S. V. Sokolovskiy, Remote sensing of refractivity from space for global observations of atmospheric parameters, *Rep. 119*, Max Planck-Inst. für Meteorologie, Hamburg, Germany, 1993.

Healy, S. B., A statistical comparison of GPS/MET radio occultation data with numerical weather prediction analyses, *Tech. Rep. 247*, 43 pp., UKMO Forecasting Research, Bracknell, UK, 1998.

Healy, S. B., and J. R. Eyre, Retrieving temperature, water vapour and surface pressure information from refractive index profiles derived by radio occultation: a simulation study, *Q. J. R. Meteorol.*

Soc., in press, 2000.

Hocke, K., Inversion of GPS meteorology data, *Ann. Geophys., 15,* 443-450, 1997.

Jazwinski, A. H., *Stochastic processes and filtering theory,* 376 pp., Academic Press, New York, USA, 1970.

Joiner, J., and A. M. da Silva, Efficient methods to assimilate remotely-sensed data based on information content, *Q. J. R. Meteorol. Soc., 124,* 1669-1694, 1998.

Joiner, J., and L. Rokke, Variational cloud-clearing with TOVS data, *Q. J. R. Meteorol. Soc., 126,* 725-748, 2000.

Kuo, Y. H., X. Zou, and W. Huang, The impact of global positioning system data on the prediction of an extratropical cyclone: an observing system simulation experiment, *Dynam. of Atm. and Oceans, 27,* 439-470, 1998.

Kursinski, E. R., G. A. Hajj, K. R. Hardy, L. J. Romans, and J. T. Schofield, Observing tropospheric water vapor by radio occultation using the global positioning system, *Geophys. Res. Lett., 22,* 2365-2368, 1995.

Kursinski, E. R., G. A. Hajj, W. I. Bertiger, S. S. Leroy, T. K. Meehan, L. J. Romans, J. T. Schofield, D. J. McCleese, W. G. Melbourne, C. L. Thornton, T. P. Yunck, J. R. Eyre, and R. N. Nagatani, Initial results of radio occultation observations of Earth's atmosphere using the global positioning system, *Science, 271,* 1107-1110, 1996.

Kursinski, E. R., G. A. Hajj, J. T. Schofield, R. P. Linfield, and K. R. Hardy, Observing Earth's atmosphere with radio occultation measurements using the global positioning system, *J. Geophys. Res., 102,* 23429-23465, 1997.

Lindal, G. F., The atmosphere of Neptune: an analysis of radio occultation data acquired with Voyager 2, *The Astron. J., 103,* 967-982, 1992.

Lindzen, R. S., and M. Fox-Rabinovitz, Consistent vertical and horizontal resolution, *Mon. Weather Rev., 117,* 2575-2583, 1989.

Matsumura, T., J. C. Derber, J. G. Yoe, F. Vandenberghe, and X. Zou, The inclusion of GPS limb

sounding into NCEP's global data assimilation system, *Office Note 426*, NOAA/NWS/NCEP, Camp Springs, Maryland, USA, 1999.

Mortensen, M. D., and P. Høeg, Inversion of GPS occultation measurements using Fresnel diffraction theory, *Geophys. Res. Lett.*, *25*, 2441-2444, 1998.

Palmer, P. I., Analysis of atmospheric temperature and humidity from radio occultation measurements, D. Phil. thesis, Oxford University, 1998.

Palmer, P. I., J. J. Barnett, J. R. Eyre, and S. B. Healy, A non-linear optimal estimation inverse method for radio occultation measurements of temperature, humidity and surface pressure, *J. Geophys. Res., in press*, 2000.

Rodgers, C. D., Retrieval of atmospheric temperature and composition from remote measurement of thermal radiation, *Rev. of Geophys. and Space Phys.*, *14*, 609-624, 1976.

Rodgers, C. D., Characterization and error analysis of profiles retrieved from remote sounding measurements, *J. Geophys. Res.*, *95*, 5587-5595, 1990.

Steiner, A. K., G. Kirchengast, and H. P. Ladreiter, Inversion, error analysis and validation of GPS/MET occultation data, *Ann. Geophys.*, *17*, 122-138, 1999.

Zou, X., F. Vandenberghe, B. Wang, M. E. Gorbunov, Y. H. Kuo, S. Sokolovskiy, J. C. Chang, J. G. Sela, R. A. Anthes, A ray-tracing operator and its adjoint for the use of GPS/MET refraction angle measurements, *J. Geophys. Res.*, *104*, 22301-22318, 1999.

P. Poli, J. Joiner Data Assimilation Office, Code 910.3 NASA Goddard Space Flight Center Greenbelt, Maryland, 20771, USA. (email: ppoli@dao.gsfc.nasa.gov; joiner@dao.gsfc.nasa.gov)

E. R. Kursinski MS 238-600 4800 Oak Grove Drive Pasadena, CA. 91109, USA. (email: erk@cobra.jpl.nasa.gov)

Received _____

[1]Joint Center for Earth Systems Technology, Baltimore, Maryland.

[2]Laboratory for Atmospheres, NASA Goddard Space Flight Center, Greenbelt, Maryland.

[3]Jet Propulsion Laboratory, California Institute of Technology, Pasadena, California.

[4]Also at Meteo France, CNRM/GMAP, Toulouse, France.

To be submitted to the *J. Geophys. Res.*, 2000.